RADIO SCIENCE, VOL. 42, RS6S15, doi:10.1029/2007RS003644, 2007

Analytical and numerical investigation of the radiation and scattering from concentric metamaterial cylinders excited by an electric line source

Samel Arslanagic,[1] Richard W. Ziolkowski,[2] and Olav Breinbjerg[1]

Received 13 February 2007; revised 14 August 2007; accepted 31 August 2007; published 15 November 2007.

[1] An antenna configuration consisting of an arbitrarily located electric line source radiating in the presence of a pair of concentric metamaterial cylinders is investigated analytically and numerically. The near- and far-field properties of these structures are analyzed through an investigation of such parameters as the total radiated power, directivity, and total as well as differential scattering cross sections. The results obtained for these metamaterial structures are compared to those for the corresponding structures made of conventional materials. It is shown that electrically small concentric metamaterial structures can be designed to be resonant and to possess advantageous radiation and scattering characteristics in contrast to the corresponding structures made of conventional materials. More specifically, it is shown that metamaterial structures lead to significant enhancements of the total radiated power as well as the total and differential scattering cross sections. Moreover, the feasibility of controlling the directivity pattern of the electrically small metamaterial structures through appropriate locations of the electric line source is demonstrated. The effects of the dispersion and loss present in the metamaterials are taken into account to study the bandwidth properties of these resonant configurations.

Citation: Arslanagic, S., R. W. Ziolkowski, and O. Breinbjerg (2007), Analytical and numerical investigation of the radiation and scattering from concentric metamaterial cylinders excited by an electric line source, *Radio Sci.*, *42*, RS6S15, doi:10.1029/2007RS003644.

1. Introduction

[2] The electromagnetics community has recently experienced a broad and intense interest in exploring and exploiting the electromagnetic characteristics and properties of various classes of metamaterials (MTMs) and combinations of these with the conventional double-positive (DPS) materials, characterized by a positive real part of both the permittivity and permeability. The different MTMs include double-negative (DNG) materials, characterized by a negative real part of both the permittivity and permeability, considered by *Veselago* [1968], and single-negative (SNG) materials, characterized by a negative real part of either the permittivity (so-called epsilon-negative (ENG) materials) or the permeability (so-called mu-negative (MNG) materials). A considerable amount of analysis to understand the properties of both DNG and SNG materials has already been performed [see *Caloz and Itoh*, 2006; *Eleftheriades and Balmain*, 2005; *Engheta and Ziolkowski*, 2006, and references therein].

[3] The increasing interest in MTMs is due to their unusual electromagnetic properties and the potential to exploit these for a variety of applications [*Caloz and Itoh*, 2006; *Eleftheriades and Balmain*, 2005; *Engheta and Ziolkowski*, 2006; *Veselago*, 1968]. Different MTM configurations have been considered, particularly canonical rectangular, cylindrical, and spherical shapes. Among the rectangular geometries, the lossless DNG slab has attracted much attention due to its so-called perfect lens property [*Pendry*, 2000]. Moreover, resonance, tunnelling, and transparency properties of DNG and SNG mono- and bi-layers have been investigated by *Caloz and Itoh* [2006], *Eleftheriades and Balmain* [2005], *Engheta and Ziolkowski* [2006], and *Alú and Engheta* [2003b]. The plane wave scattering properties of MTM cylinders and spheres, as well as their radiation properties when illuminated by more realistic sources of radiation, such as Hertizan dipoles and line sources have

[1]Ørsted·DTU, ElectroScience, Technical University of Denmark, Lyngby, Denmark.
[2]Department of Electrical and Computer Engineering, University of Arizona, Tucson, Arizona, USA.

0048-6604/07/2007RS003644$11.00

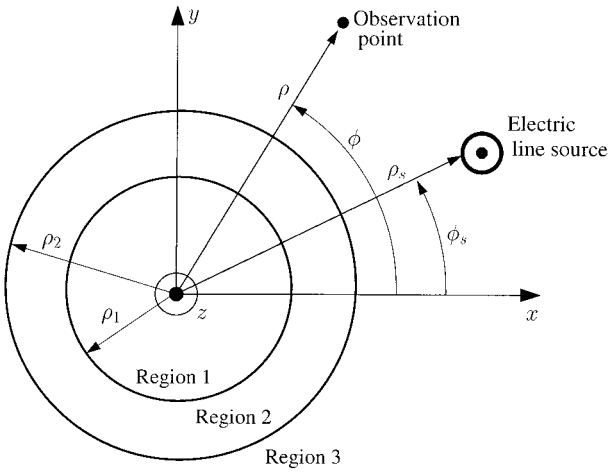

Figure 1. Configuration of the ELS-excited concentric pair of MTM cylinders.

been investigated in detail [*Caloz and Itoh*, 2006; *Eleftheriades and Balmain*, 2005; *Engheta and Ziolkowski*, 2006; *Arslanagic and Breinbjerg*, 2006; *Arslanagic et al.*, 2006a, 2006b, 2006c, 2006d, 2006e, 2007; *Alú and Engheta*, 2003a, 2005; *Engheta and Alú*, 2005; *Khodier*, 2004; *Kuzmiak and Maradudin*, 2002; *Li and Shen*, 2003; *Liu et al.*, 2004; *Nelatury*, 2006; *Ruppin*, 2000, 2004; *Sun et al.*, 2005; *Tretyakov et al.*, 2005; *Ziolkowski and Erentok*, 2006, 2007; *Ziolkowski and Kipple*, 2003, 2005]. In particular, it has been demonstrated that electrically small MTM cylindrical or spherical shells can be designed to produce resonant configurations [*Arslanagic et al.*, 2006a, 2006b, 2006c, 2006d, 2006e, 2007; *Alú and Engheta*, 2003a, 2005; *Caloz and Itoh*, 2006; *Eleftheriades and Balmain*, 2005; *Engheta and Ziolkowski*, 2006; *Liu et al.*, 2004; *Ziolkowski and Erentok*, 2006, 2007; *Ziolkowski and Kipple*, 2003] which lead to significant enhancements of the total radiated power, as well as the total scattering cross section.

[4] The purpose of the present work is to further investigate the radiation and scattering from electrically small resonant concentric MTM cylinders illuminated by an electric line source (ELS). (The ELS type of illumination corresponds to TM polarization. The results for the magnetic line source illumination, which correspond to TE polarization, are readily obtained by duality and these are thus not included here.) In distinction to related efforts which have investigated the properties of multilayered concentric cylindrical structures excited by an ELS located at their origin [e.g., *Tretyakov et al.*, 2005], the present work allows the ELS to be arbitrarily located. More specifically, it is shown that the use of MTMs in such electrically small structures leads to significant enhancement of the total radiated power, as compared to the power radiated by the source into free space. Moreover, it is shown that in the case of the ELS being infinitely far from the cylinders, the total and differential scattering cross section are likewise significantly enhanced when MTMs are used, as compared to the results obtained for the corresponding cylinders composed of only DPS materials. Furthermore, the feasibility of controlling the directivity of the electrically small MTM structures by appropriate alternation of the ELS location is demonstrated; and its use in the design of directive electrically small antennas is discussed.

[5] The present manuscript is organized as follows. In section 2, the analytical solution to the problem of an arbitrarily located ELS radiating in the presence of a concentric pair of MTM cylinders is derived, and the figures of merit, used in the subsequent numerical results are defined. In section 3, the condition for resonance is derived and discussed. Furthermore, some important differences between electrically small two-dimensional (2D) and three-dimensional (3D) structures are emphasized. Moreover, the present results regarding the enhanced radiation characteristics with resonant MTM cylindrical structures are related to those by *Tretyakov et al.* [2005], where similar configurations have been examined. In section 4, the numerical results, including the near field, directivity, total and differential cross sections, are shown for some specifically designed electrically small structures. In particular, the so-called dipolar and quadrupolar structures, to be defined in section 4, will be investigated. In order to study the bandwidth properties of the resonant configurations identified in section 4, the effects of dispersion are taken into account in section 5, which moreover includes the analysis of the effects of losses in MTMs. Furthermore, the fundamental distinctions between the resonant electrically small structures and those for which the resonant behavior is related to the overall size of the structure are pointed out in section 6. Finally, in section 7, the use of SNG media in the design of electrically small resonant structures is briefly discussed. Throughout this manuscript, the time factor $\exp(j\omega t)$, with ω being the angular frequency and t being the time, is assumed and suppressed.

2. Analytical Solution

[6] The cross section of the 2D configuration of interest is depicted in Figure 1. A circular cylindrical core of radius ρ_1 (region 1) is covered with a concentric cylindrical shell of outer radius ρ_2 (region 2) and imbedded in an infinite ambient medium (region 3). The structure is illuminated by an infinite ELS of a constant electric current I_e. The axes of the cylinders and

the ELS are parallel, and the ELS can be located in any of the three regions. Region i, with i = 1 and 2, is characterized by a permittivity and a permeability, denoted by $\varepsilon_i = \varepsilon_i' - j\varepsilon_i''$ and $\mu_i = \mu_i' - j\mu_i''$, respectively, and a wave number denoted by $k_i = \omega\sqrt{\varepsilon_i\mu_i}$, where the branch of the square root is chosen so that $\mathrm{Im}\{k_i\} \leq 0$. Each of these regions can be composed of simple DPS, DNG, or SNG materials. The exterior region, region 3, is free space with the permittivity ε_0 and permeability μ_0, and thus the wave number $k_0 = \omega\sqrt{\varepsilon_0\mu_0}$ and intrinsic impedance $\eta_0 = \sqrt{\mu_0/\varepsilon_0}$. A cylindrical coordinate system (ρ, ϕ, z) and the associated Cartesian coordinate system (x, y, z) are introduced such that the z-axis coincides with the axis of the cylinders. The coordinates of the observation point are (ρ, ϕ), while the coordinates of the ELS are (ρ_s, ϕ_s).

[7] Using the cylindrical wave functions with origins at ρ = 0, the electric field generated by the ELS in an infinite medium characterized by ε_{ELS}, μ_{ELS}, and k_{ELS} is given by the well-known expression [*Balanis*, 1989, chapter 11]

$$\vec{E}_{ELS}(\rho,\varphi) = -\hat{z}I_e\frac{\omega\mu_{ELS}}{4}\begin{cases}\displaystyle\sum_{n=0}^{N_{\max}}\tau_n J_n(k_{ELS}\rho)H_n^{(2)}(k_{ELS}\rho_s)\cos[n(\varphi-\varphi_s)] & \text{for} \quad \rho \leq \rho_s,\\ \displaystyle\sum_{n=0}^{N_{\max}}\tau_n J_n(k_{ELS}\rho_s)H_n^{(2)}(k_{ELS}\rho)\cos[n(\varphi-\varphi_s)] & \text{for} \quad \rho \geq \rho_s,\end{cases} \tag{1}$$

where $J_n(\cdot)$ is the Bessel function of order n and is chosen to represent the field for $\rho \leq \rho_s$ since it is finite at the origin, while $H_n^{(2)}(\cdot)$ is the Hankel function of second kind and order n, and is chosen for $\rho \geq \rho_s$ because it represents an outward propagating wave that complies with the radiation condition. The symbol τ_n is the Neumann number; i.e., τ_n = 1 for n = 0, and τ_n = 2 otherwise. Furthermore, $N_{\max}$ is the truncation limit in the numerical implementation of the infinite summation in the exact solution, chosen to ensure the convergence of this expansion. It is noted that $\varepsilon_{ELS} = \varepsilon_i$, $\mu_{ELS} = \mu_i$, and $k_{ELS} = k_i$, i = 1 and 2, respectively, when the ELS is in region 1 and 2, while $\varepsilon_{ELS} = \varepsilon_0$, $\mu_{ELS} = \mu_0$, and $k_{ELS} = k_0$ when the ELS is in region 3. The field $\vec{E}_{ELS}$ in (1) constitutes the known incident field for the scattering problem shown in Figure 1.

[8] The unknown fields in each of the regions (i.e., the scattered field in the region containing the ELS and the total fields in the other regions) are likewise expanded in terms of cylindrical wave functions, and these can thus be expressed as

$$\vec{E}_{1s}(\rho,\phi) = -\hat{z}I_e\frac{\omega\mu_1}{4}\sum_{n=0}^{N_{\max}}\tau_n C_{1n}J_n(k_1\rho) \cdot \cos[n(\phi-\phi_s)] \text{ for } \rho \leq \rho_1, \tag{2a}$$

$$\vec{E}_{2s}(\rho,\phi) = -\hat{z}I_e\frac{\omega\mu_2}{4}\sum_{n=0}^{N_{\max}}\tau_n[C_{2n}J_n(k_2\rho) + C_{3n}Y_n(k_2\rho)] \cdot \cos[n(\phi-\phi_s)] \text{ for } \rho_1 \leq \rho \leq \rho_2, \tag{2b}$$

$$\vec{E}_{3s}(\rho,\phi) = -\hat{z}I_e\frac{\omega\mu_0}{4}\sum_{n=0}^{N_{\max}}\tau_n C_{4n}H_n^{(2)}(k_0\rho) \cdot \cos[n(\phi-\phi_s)] \text{ for } \rho \geq \rho_2, \tag{2c}$$

where C_{in}, with i = 1, . . ., 4 and n = 0, 1, 2, . . ., $N_{\max}$, are the unknown expansion coefficients and $Y_n(\cdot)$ is the Neumann function of order n. The expressions (1) and (2) represent multipole expansions of the fields, e.g., the n = 0 term corresponds to the monopolar mode, the n = 1 term corresponds to the dipolar mode, the n = 2 term corresponds to the quadrupolar mode, etc. The corresponding magnetic fields, which are required for the determination of the unknown expansion coefficients, are readily obtained from Faraday's law. Enforcing the electromagnetic field boundary conditions, i.e., requiring the tangential components of the electric and magnetic fields to be continuous at the interfaces at $\rho = \rho_1$ and $\rho = \rho_2$, it follows that the unknown expansion coefficients can be found from the following matrix equation,

$$\vec{C}_n = \overline{\overline{\mathrm{M}}}_n^{-1}\vec{\Lambda}_n, \qquad n = 0, 1, 2, \ldots N_{\max} \tag{3}$$

where $\vec{C}_n = [C_{1n}, C_{2n}, C_{3n}, C_{4n},]$ is the vector containing the four unknown expansion coefficients for the n'th term, and $\vec{\Lambda}_n = [\Lambda_{1n}, \Lambda_{2n}, \Lambda_{3n}, \Lambda_{4n},]$ is the excitation vector which depends on the location of the ELS. The elements of this excitation vector are shown in Table 1.

[9] The matrix $\overline{\overline{\mathrm{M}}}_n$ is a four-by-four matrix that depends on the values of the cylindrical waves at the two interfaces, and it is given by

$$\overline{\overline{\mathrm{M}}}_n = \begin{bmatrix} -\mu_1 J_n(k_1\rho_1) & \mu_2 J_n(k_2\rho_1) & \mu_2 Y_n(k_2\rho_1) & 0 \\ -k_1 J_n'(k_1\rho_1) & k_2 J_n'(k_2\rho_1) & k_2 Y_n'(k_2\rho_1) & 0 \\ 0 & \mu_2 J_n(k_2\rho_2) & \mu_2 Y_n(k_2\rho_2) & -\mu_3 H_n^{(2)}(k_0\rho_2) \\ 0 & k_2 J_n'(k_2\rho_2) & k_2 Y_n'(k_2\rho_2) & -k_3 H_n^{(2)\prime}(k_0\rho_2) \end{bmatrix}. \tag{4}$$

Table 1. Elements Λ_{in}, i = 1, 2, 3, and 4, of the Excitation Vector $\vec{\Lambda}_n$ When the ELS Is Located in Regions 1, 2, or 3

Λ_{in}	ELS in Region 1	ELS in Region 2	ELS in Region 3
Λ_{1n}	$\mu_1 J_n(k_1\rho_s)$ $H_n^{(2)}(k_1\rho_1)$	$-\mu_2 J_n(k_2\rho_1)$ $H_n^{(2)}(k_2\rho_s)$	0
Λ_{2n}	$k_1 J_n(k_1\rho_s)$ $H_n^{(2)\prime}(k_1\rho_1)$	$-k_2 J_n'(k_2\rho_1)$ $H_n^{(2)}(k_2\rho_s)$	0
Λ_{3n}	0	$-\mu_2 J_n(k_2\rho_s)$ $H_n^{(2)}(k_2\rho_2)$	$\mu_0 J_n(k_0\rho_2)$ $H_n^{(2)}(k_0\rho_s)$
Λ_{4n}	0	$-k_2 J_n(k_2\rho_s)$ $H_n^{(2)\prime}(k_2\rho_2)$	$k_0 J_n'(k_0\rho_2)$ $H_n^{(2)}(k_0\rho_s)$

In the above expressions, the prime denotes the derivative with respect to the entire argument.

[10] The figures of merit to be employed in the subsequent numerical investigation are the total radiated power, the two-dimensional directivity, and the total as well as the differential scattering cross section, where the latter two parameters are evaluated in the case where the ELS is moved infinitely far away from the concentric cylinders. Henceforth, these quantities are referred to as simply the total power, the directivity, and the total and differential cross sections, respectively. Since the configuration is infinite in the z -direction, all of the quantities are determined on a per unit length basis.

[11] The total power, denoted by P_t, is given by the expression

$$P_t = \lim_{\rho\to\infty} \frac{1}{2\eta_0} \int_{\varphi=0}^{2\pi} \left|\vec{E}_t(\rho,\phi)\right|^2 \rho d\phi, \tag{5}$$

where $\vec{E}_t$ denotes the total field in region 3. This equals either the sum of the field in (1) for $\rho \geq \rho_s$ and the field (2c) for region 3 when the ELS is in region 3, or it equals the field (2c) for region 3 when the ELS is located in either region 1 or 2. The relevant expression for the total field in (5) is easily obtained by introducing the large argument approximation of the Hankel function [*Abramowitz and Stegun*, 1965, chapter 10]. The resulting expression for the total power thus becomes

$$P_t = \left(\frac{1}{4}\eta_0 I_e^2\right)\left[\frac{k_0}{4}\sum_{n=0}^{N_{\max}} \tau_n^2(3-\tau_n)|\alpha_n|^2\right], \tag{6}$$

where $\alpha_n = J_n(k_0\rho_s) + C_{4n}$ when the ELS is located in region 3, and $\alpha_n = C_{4n}$ when the ELS is located in either region 1 or 2. The power radiated by the ELS alone in free space, denoted by P_i, is given by (5) with $\vec{E}_t$ replaced by $\vec{E}_{ELS}$ in (1) for $\rho \geq \rho_s$. In this case, $N_{\max}$ can be set to infinity and it is found that

$$\begin{aligned} P_i &= \left(\frac{1}{4}\eta_0 I_e^2\right)\left[\frac{k_0}{4}\sum_{n=0}^{N_{\max}} \tau_n^2(3-\tau_n)|J_n(k_0\rho_s)|^2\right]_{N_{\max}=\infty} \\ &= \left(\frac{1}{4}\eta_0 I_e^2\right)\left[\frac{k_0}{2}\right], \end{aligned} \tag{7}$$

where the sum has been evaluated using the well-known result found in, e.g., the work of *Abramowitz and Stegun* [1965, chapter 10]. Of particular interest to the current investigation is the comparison of the total power in the presence of the concentric MTM cylinders to that radiated by the ELS alone. To this end, the so-called power ratio (PR) is introduced and this is given by

$$\mathrm{PR} = \frac{P_t}{P_i} = \frac{1}{2}\sum_{n=0}^{N_{\max}} \tau_n^2(3-\varepsilon_n)|\alpha_n|^2. \tag{8}$$

[12] The directivity, D, is given by

$$\begin{aligned} D(\phi) &= \lim_{\rho\to\infty} \frac{2\pi\rho\left|\vec{E}_t(\rho,\phi)\right|^2}{\int_{\varphi=0}^{2\pi}\left|\vec{E}_t(\rho,\phi)\right|^2\rho d\phi} \\ &= \frac{2\left|\sum_{n=0}^{N_{\max}} \tau_n j^n \alpha_n \cos[n(\phi-\phi_s)]\right|^2}{\sum_{n=0}^{N_{\max}} \tau_n^2(3-\varepsilon_n)|\alpha_n|^2}. \end{aligned} \tag{9}$$

[13] In the case where the ELS location is moved infinitely far away in region 3, i.e., for $\rho_s \to \infty$, it is moreover of interest to investigate the behavior of the differential and total cross section of the cylinders. The differential cross section, defined by the square of the ratio of the magnitude of the scattered far-field (in region 3) to the magnitude of the incident field at the origin, evaluated when the ELS is moved infinitely far away from the cylinders along an arbitrary direction ϕ_s, is given by

$$\begin{aligned} \sigma_d &= \lim_{\rho\to\infty}\lim_{\rho_s\to\infty;\phi_s}\left[2\pi\rho\frac{\left|\vec{E}_{3s}(\rho,\phi)\right|^2}{\left|\vec{E}_{ELS}(\rho=0)\right|^2}\right] \\ &= \frac{4}{k_0}\left|\sum_{n=0}^{N_{\max}} \tau_n C_{4n}'(-1)^n \cos[n(\phi-\phi_s)]\right|^2, \end{aligned} \tag{10}$$

with the coefficient $C_{4n}' = C_{4n}/H_n^{(2)}(k_0\rho_s)$, where C_{4n} has been defined previously. Thus the coefficient C_{4n}' is obtained as a solution of (3), i.e., the same equation which yields C_{4n}, except for the fact that the term

$H_n^{(2)}(k_0\rho_s)$, which is contained in the excitation vector when the ELS is in region 3, see Table 1, has now been cancelled out.

[14] The total cross section, σ_t, defined by the ratio of the power, P_s, contained in the scattered far field to the incident power density, S_i, at the origin, again evaluated when the ELS is moved infinitely far away from the cylinders (i.e., for $\rho_s \to \infty$) along an arbitrary direction ϕ_s, is given by

$$\sigma_t = \lim_{\rho_s\to\infty;\phi_s} \frac{P_s}{S_i} = \lim_{\rho\to\infty} \lim_{\rho_s\to\infty;\phi_s} \frac{\int_{\varphi=0}^{2\pi} \left|\vec{E}_{3s}(\rho,\phi)\right|^2 \rho d\phi}{\left|\vec{E}_{ELS}(\rho=0)\right|^2} = \frac{2}{k_0}\sum_{n=0}^{N_{\max}} \tau_n^2(3-\varepsilon_n)\left|C'_{4n}\right|^2. \quad (11)$$

[15] When the ELS is moved infinitely far away from the concentric cylinders, the incident field generated by the ELS constitutes locally a plane wave. Thus, the cross sections in (10) and (11) recover the usual plane wave cross sections.

[16] Numerical results for the above figures of merit are presented and discussed in the following section. It is understood that while the ELS and concentric MTM cylinders can be considered as a radiating system when the ELS is located in regions 1 and 2, as well as when it is located in region 3 at moderate distances from the structure, it can be considered as a scattering system when the ELS is moved infinitely far way from the cylinder. Thus, both the radiating and scattering properties of the structures will be investigated. Throughout the following investigations, a structure is referred to by its properties in region 1 and 2. For instance, a DPS-MTM structure, where the MTM can be either a DNG, ENG, or MNG material, indicates that region 1 consists of a DPS material while region 2 consists of the selected MTM. However, in the majority of the following cases, DPS and DNG materials are employed.

3. Resonance Condition: Derivation and Discussion

[17] In order to provide more insight into the physics associated with the electrically small resonant cylindrical structures, it is useful to first find the conditions for which the enhancements of the total power, total and differential cross sections will occur. Since both the total power (6) and the cross sections (10) and (11) are proportional to $|C_{4n}|^2$, large values of these quantities will result if the amplitude of the expansion coefficient C_{4n} is large. Such large values of the expansion coefficients are related to the presence of the so-called natural modes, and the corresponding peaks in the expansion coefficients are referred to as natural resonances [see, e.g., *Alú and Engheta*, 2003a, 2005; *Engheta and Ziolkowski*, 2006; *Ziolkowski and Kipple*, 2005, and references therein]. When the structure of interest is composed of DPS materials, the natural resonances occur only if the size of the structures is on the order of, or larger than, the wavelength inside the material [*Alú and Engheta*, 2003a, 2005; *Engheta and Ziolkowski*, 2006; *Ziolkowski and Kipple*, 2005]. These wavelength-sized natural resonances will be discussed briefly in section 6. However, when the structure is composed of combinations of DPS, DNG, and/or SNG materials, the scattering coefficients may exhibit peaks, and thus resonances, even if the structures are significantly smaller than the wavelength, and such resonances are attributed to the clever pairing of DPS, DNG, and/or SNG materials [*Alú and Engheta*, 2003a, 2005; *Engheta and Ziolkowski*, 2006; *Ziolkowski and Kipple*, 2005]. In the works of *Alú and Engheta* [2003a], *Engheta and Ziolkowski* [2006], and *Alú and Engheta* [2005], these resonances are referred to as interface resonances, but here they are designated as subwavelength-sized natural resonances.

[18] To find the condition for which the amplitudes of the expansion coefficient C_{4n} become large, one first notes that, according to (3), these are proportional to the product of the inverse of the matrix $\overline{\overline{\mathrm{M}}}_n$ and the excitation vector $\vec{\Lambda}_n$. Thus, C_{4n} is inversely proportional to the determinant of $\overline{\overline{\mathrm{M}}}_n$. When the magnitude of this determinant attains a minimum, the amplitude of C_{4n} becomes large, and a resonance occurs, thus leading to enhancements of the total power and the total and differential cross sections. Since the structures are electrically small, the small argument expansions of the functions contained in $\overline{\overline{\mathrm{M}}}_n$, which hold when the products $|k_1|\rho_1$, $|k_2|\rho_1$, $|k_2|\rho_2$, and $k_0\rho_2$ are much smaller than unity, are used to derive an approximate analytical expression for the resonance condition. It must be stressed that such a derivation is greatly facilitated by assuming the materials in the three regions to be lossless. For the range of parameters to be investigated here, and with the assumption of lossless materials in regions 1 and 2, it can be shown that the C_{in} exhibits a resonance when the approximate condition

$$\frac{\rho_1}{\rho_2} \approx \sqrt[2n]{\frac{(\mu_2+\mu_1)(\mu_2+\mu_0)}{(\mu_2-\mu_1)(\mu_2-\mu_0)}}, \qquad n \geq 1 \quad (12)$$

is met. This condition is used here to determine, for a given set of material parameters, the approximate ratio of ρ_1 and ρ_2 that yields a resonant concentric pair of lossless MTM cylinders. (The adjective lossless is omitted in the following discussion. The influence of losses is taken

into account in section 5.) The resonance condition given by (12) depends on the mode number, n, a careful choice of material parameters, and only on the ratio of the inner and outer radii of region 2, and thus not on how small either of these radii are individually. Moreover, it is independent of the frequency in the sense that a resonance is attained for all frequencies for which a given set of material and geometrical parameters make the structure electrically small. In order to define a given resonant structure on the basis of (12) one can start by selecting its material parameters and its inner (outer) radius. The condition in (12) is then used to determine the outer (inner) radius for a given mode number n. Consequently, this mode will be the dominant mode excited in this structure. It is worth emphasizing that (12) holds for $n \geq 1$ and that for the range of parameters to be investigated here, the monopolar mode does not show a resonant behavior. This implies that there is no electrically small monopolar structure that will have a resonance. The relation (12) is identical to the one obtained by *Alú and Engheta* [2003a, 2005] for plane wave scattering from similar cylindrical structures. Though certain small terms have been neglected in the derivation of (12), this condition constitutes a very accurate approximation for the radii ratio at resonance, as will be demonstrated numerically below. Therefore, the expression (12) serves as a guideline to estimate the resonant configuration, i.e., as a starting point for the numerical analysis. The resonance condition in (12), which for the TM polarization investigated here is independent of the permittivities of the different regions, requires that at least one of the parameters μ_1 or μ_2 is negative. In particular, it can be shown that (12) is satisfied for either of the following three cases,

(a) $\mu_1 > 0$ and $\mu_2 < 0$ if $|\mu_2| < \min(\mu_1, \mu_0)$ or $|\mu_2| > \max(\mu_1, \mu_0)$,

(b) $\mu_1 < 0$ and $\mu_2 > 0$ if $\mu_2 > |\mu_1| > \mu_0$ or $\mu_2 < |\mu_1| < \mu_0$,

(c) $\mu_1 < 0$ and $\mu_2 < 0$ if $|\mu_2| > \mu_0 > |\mu_1|$ or $|\mu_2| < \mu_0 < |\mu_1|$.

The DPS-DNG structures are emphasized in the following discussions, while a brief account on the use of SNG materials will be made in section 7.

[19] An interesting observation for the configurations in which the ELS is located in region 1 along the axis of the cylinders, i.e., in which $\rho_s = 0$, can now be made. From Table 1 it is understood that the nonzero elements of the excitation vector $\vec{\Lambda}_n$ for the ELS in region 1 are proportional to $J_n(k_1\rho_s)$. Since $J_n(0) = 0$ for $n > 0$, only $C_{i0} \neq 0$ and, thus, only the monopolar mode radiates when the ELS is located on the axis of the cylinders. In particular, according to the discussion following (12), there is no electrically small monopolar resonant structure for the range of parameters to be investigated here. Consequently, one concludes that the resonances associated with the excitation of higher-order modes ($n = 1, 2, 3, \ldots$) in the electrically small concentric MTM cylinders occur only if the ELS is located off the cylinder axis, i.e., for $\rho_s > 0$. These observations highlight one of the most important differences between the electrically small 2D and 3D structures since the latter lead to resonances when the source is located at the origin [*Ziolkowski and Erentok*, 2006, 2007; *Ziolkowski and Kipple*, 2005]. Moreover, the present findings for the $\rho_s = 0$ case are in agreement with *Tretyakov et al.* [2005], where it was noted that such 2D configurations do not affect the field distributions or the power radiated by the ELS. Therefore, the assumption that the ELS is located at the origin, as was done by *Tretyakov et al.* [2005], clearly limits the analysis to considerations of only monopolar cases, which are nonresonant for electrically small structures. However, as demonstrated below, the 2D DPS-DNG configurations with $\rho_s > 0$ can lead to the excitement of the higher order resonances and, hence, to an enhancement of, e.g., the total power radiated by the ELS when it is situated close to (or surrounded by) the structure. This behavior is obviously in sharp contrast to the $\rho_s = 0$ case. The presence of resonances in several DPS-DNG structures and their absence in the corresponding DPS-DPS cases will be demonstrated below. Furthermore, as reported by *Khodier* [2004] and *Nelatury* [2006] and as demonstrated additionally in section 6, the larger cylindrical structures exhibit resonances for both the DPS-DPS and DPS-DNG cases when the ELS is located at the center of the cylinders.

4. Numerical Results

4.1. Resonant Configurations: Definition

[20] The material and geometrical parameters selected to illustrate the results for the electrically small resonant structures are summarized in Table 2. Regions 1 and 3 are chosen to be free space, while region 2 is taken to be a DNG material. For these fixed material parameters, the condition in (12) was used to define the approximate geometrical parameters that produce the resonant dipolar and quadrupolar modes. The associated structures are referred to as the resonant dipolar and quadrupolar structures, respectively. The positive material parameters in region 2 of the corresponding DPS-DPS structures are also indicated in Table 2. Thus, the structures under examination are either a DNG or a DPS cylindrical shell in the presence of an ELS, which can be located in any of the three regions. Throughout these investigations the frequency of operation is $f_0 = 300$ MHz, implying that

Table 2. Material and Approximate Geometrical Parameters for Region 2 of the Electrically Small Resonant Dipolar and Quadrupolar Configurations[a]

Structure	ε_2	μ_2	ρ_1, mm	ρ_2, mm
Dipolar	$\pm\varepsilon_0$	$\pm 4\mu_0$	6	10
Quadrupolar	$\pm\varepsilon_0$	$\pm 4\mu_0$	3.8729	5

[a]Positive values of the material parameters indicate a DPS material, while negative values indicate a DNG material.

the free-space wavelength is $\lambda_0 = 1$ m. Note that the numerical code was used to determine the precise radii at which the resonance is achieved.

[21] From relation (12) and Table 2 it follows that for fixed material parameters a considerably thinner structure is needed to excite the quadrupolar mode than the dipolar mode. One also notes that the diameter of the resonant dipolar structure is 20 mm, or $\lambda_0/50$ (which corresponds to $k_0\rho_2 = 0.063$), while that of the quadrupolar structure is 10 mm, or $\lambda_0/100$ (which corresponds to $k_0\rho_2 = 0.032$).

4.2. Electrically Small Dipolar Structures

[22] The electrically small resonant dipolar DPS-DNG structure defined in section 4.1 is examined with respect to its radiation and scattering properties. Furthermore, it is compared to the corresponding DPS-DPS structure.

4.2.1. Total Power

[23] Figure 2 shows the PR for the dipolar DPS-DNG and DPS-DPS structures as a function of the outer radius ρ_2, when the inner radius is fixed at $\rho_1 = 6$ mm. The ELS is located in region 1 at $\rho_s = 5.99$ mm. The ELS is located near the interface of the DPS and DNG layers because it produces the largest peak value of the PR.

[24] For the DPS-DNG structure, a resonance peak (of value PR $\approx$ 23 dB or PR $\approx$ 200) is found for $\rho_2 = 10.03$ mm, which is very close to the approximate value of 10 mm obtained from (12). The PR values for the corresponding DPS-DPS structure are also given in Figure 2. In contrast to the DPS-DNG structure, no resonances are observed for this DPS-DPS structure, where the PR is very close to unity. Similar results, not included here, have been obtained for DPS-DNG and DPS-DPS dipolar structures when the ELS is located in region 2 or 3.

[25] To demonstrate the influence of the ELS location on the resonant enhancements of the total power, Figures 3a–3c show the PR as a function of the ELS position, ρ_s, with the ELS in regions 1, 2, and 3, respectively, for the DPS-DNG and DPS-DPS structures having the fixed radii: $\rho_1 = 6$ mm and $\rho_2 = 10.03$ mm. In particular, the ELS location varies in the interval $\rho_s \in [1-5.99]$ mm in Figure 3a, in $\rho_s \in [6.01-9.99]$ mm for Figure 3b, and in $\rho_s \in [10.1-25]$ mm for Figure 3c.

[26] In all cases and regardless of the location of the ELS, the DPS-DPS structures offer no enhancement, i.e., the PR value is close to unity. In contrast, the corresponding DPS-DNG structures offer very large PR values, this being particularly true when the ELS is close to the surface of the DNG shell.

[27] For increasing ρ_s values in region 1, the PR increases from approximately zero to approximately 23 dB. The fact that there is no enhancement when the ELS is near the origin confirms the previous observation that the ELS must be offset from the axis to excite, in this case, the resonant dipolar mode. As the near-field investigations discussed below will confirm, the monopolar mode is dominant for small values of ρ_s.

[28] For the ELS in region 2, the largest PR values are obtained when the ELS is close to the interfaces at ρ_1 and ρ_2. However, the behavior of the PR is particularly interesting because it exhibits a minimum for a specific ELS position. This minimum occurs at $\rho_s = 7.746$ mm where the total power radiated by the ELS in the presence of the DNG shell is actually slightly lower than the power radiated by the ELS alone. As the ELS is moved in the DNG region, it is found that its ability to excite the resonant dipolar mode changes. In particular, for the minimum PR location value, it is found that the ELS couples only to the monopolar mode, a fact that will likewise be confirmed via the near-field results given below. Since the ELS can not couple to the dipolar mode,

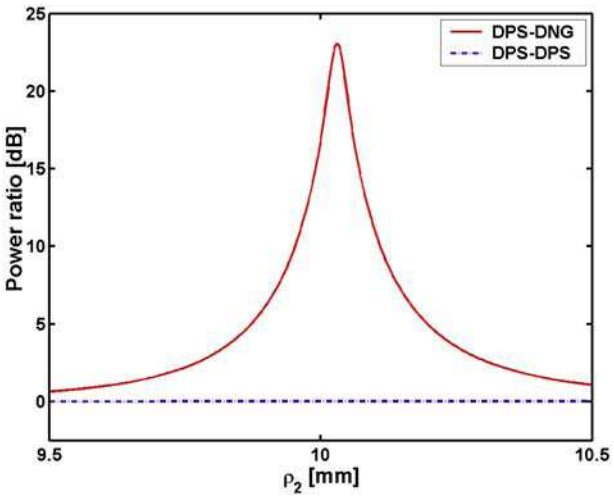

Figure 2. PR as a function of the outer shell radius ρ_2 for the DPS-DNG and DPS-DPS dipolar structures with $\rho_1 = 6.0$ mm when the ELS is located in region 1 at $\rho_s = 5.99$ mm [from *Arslanagic et al.*, 2006e]. Copyright © 2006 Wiley Periodicals, Inc.

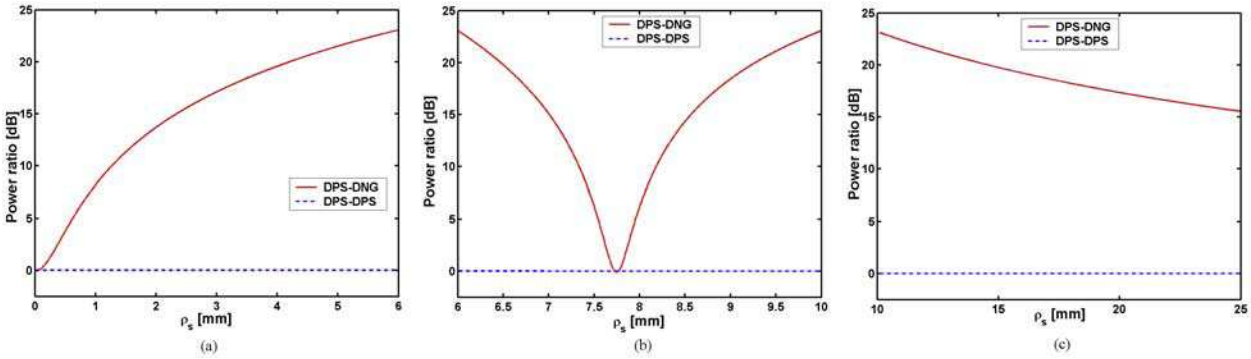

Figure 3. Power ratio as a function of the ELS location ρ_s for the DPS-DNG and DPS-DPS dipolar structures when the ELS is located in (a) region 1, (b) region 2, and (c) region 3 [from *Arslanagic et al.*, 2006e]. Copyright © 2006 Wiley Periodicals, Inc.

it can not cause a resonant enhancement of the total power. In addition to these findings, it is interesting to note that the PR is considerably less sensitive with respect to the position of the ELS than it is to the outer radius of the MTM layer. For the ELS being located in region 3, the PR is slowly decreasing for increasing ρ_s values.

4.2.2. Near Field

[29] Next, the above findings are elucidated with near-field investigations. For all of the following near-field plots, the total electric near field, denoted by $\vec{E}(\rho, \varphi)$, or more specifically, the quantity $20\log_{10}|\vec{E}(\rho, \varphi)|$, where $\vec{E}(\rho, \varphi)$ has been normalized by 1 V/m, is shown in a circular region of radius $3\rho_2$ centered at the cylinder axis (z-axis). Figure 4a shows the near field of the ELS located in free space, while Figure 4b shows the near field of the DPS-DPS structure. In both cases the ELS is located at $\rho_s = 1$ mm.

[30] As can be observed, the field radiated by the ELS in free space is, of course, of the monopolar form. The near field in Figure 4b is very similar to the one depicted in Figure 4a. This implies that the DPS-DPS structure practically does not influence the radiation from the ELS. Consequently, the electrically small DPS-DPS structure is not expected to lead to any enhancement of the desired quantities, e.g., the total power, this being in line with the behavior of the DPS-DPS structure observed in Figures 2 and 3. Similar near-field results, not included here, for the DPS-DPS structure are obtained for other locations of the ELS in regions 1, 2, and 3.

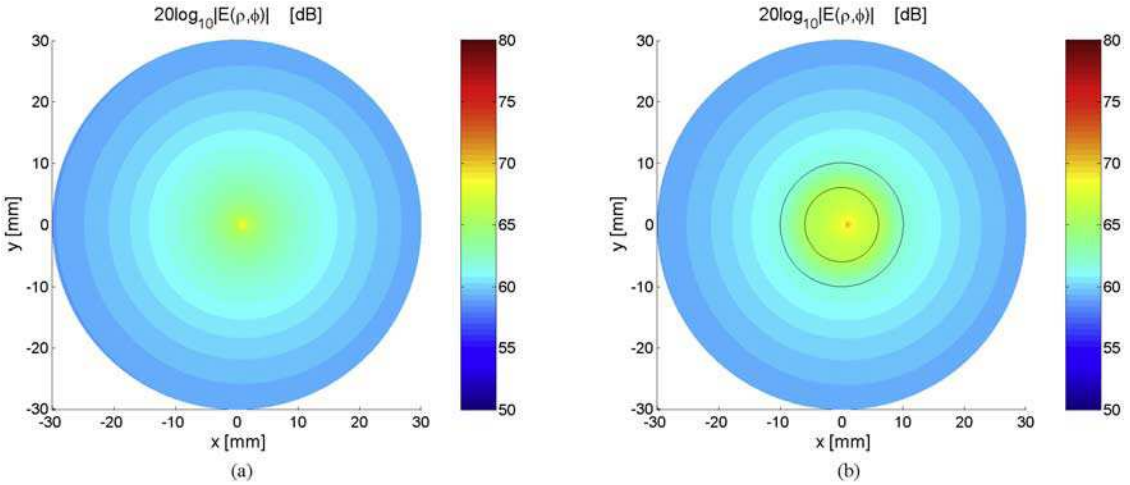

Figure 4. Electric near field of the ELS (a) in free space and (b) of the DPS-DPS structure. In both cases, the ELS is located at $\rho_s = 1$ mm. Curves representing the cylindrical surfaces of the DPS-DPS structure are also shown in Figure 4b.

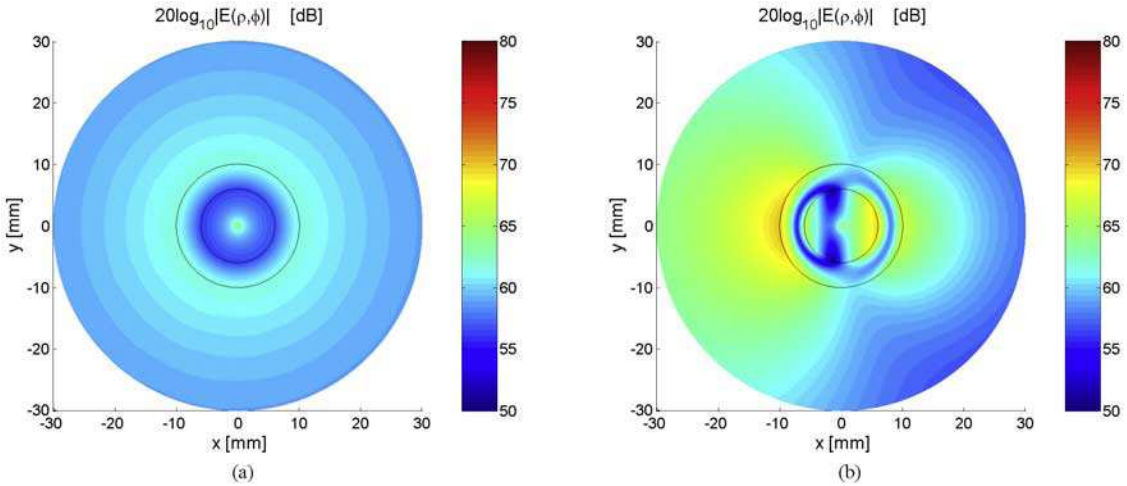

Figure 5. Electric near field of the resonant dipolar DPS-DNG structure. The ELS is located at (a) ρ_s = 0.001 mm and (b) ρ_s = 0.125 mm. Curves representing the cylindrical surfaces of the structure are also shown.

[31] The near fields for the resonant dipolar DPS-DNG structure are depicted in Figures 5 and 6. When the ELS is located at ρ_s = 0.001 mm, the near field has the monopolar form observed in Figure 5a. This confirms that for locations of the ELS close to the origin, the monopolar mode is indeed the dominant one, and thus, that no enhancement of the total power is expected for such ELS locations. This is in agreement with the previous statements regarding the necessity of exciting the higher order modes in order to obtain an enhancement. This also means that for these ELS locations, the field radiated by the ELS is not significantly affected by the presence of the DPS-DNG structure. However, as the ELS is moved just slightly away from the origin to ρ_s = 0.125 mm, the monopolar mode is mixed with the dipolar mode, as confirmed by Figure 5b. Moving the ELS even further from the origin, e.g., to ρ_s = 1 mm, leads to the near field shown in Figure 6a, which is clearly dominated by the dipolar mode. At this ELS location, an enhancement of the total power of about 8 dB is in evidence in Figure 3a. As is apparent in Figure 6, these dipolar mode enhancements become even more

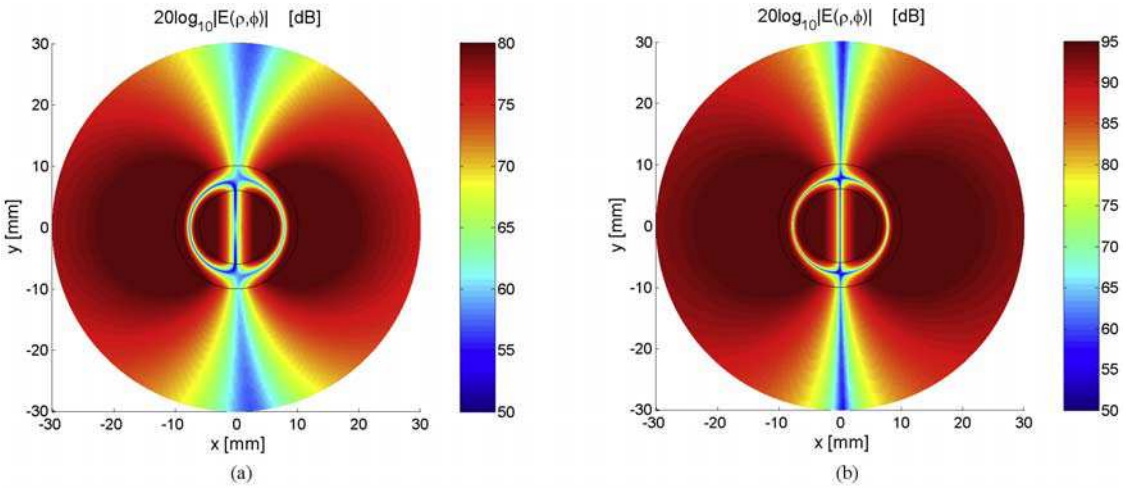

Figure 6. Electric near field of the resonant dipolar DPS-DNG structure. The ELS is located at (a) ρ_s = 1 mm and (b) ρ_s = 5.99 mm. Note that the dynamic range in Figure 6b is larger than the one in Figure 6a. Curves representing the cylindrical surfaces of the structure are also shown.

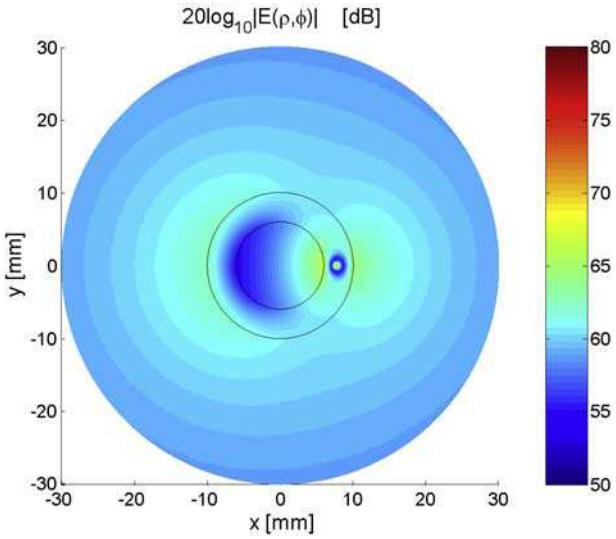

Figure 7. Electric near field of the resonant dipolar DPS-DNG structure. The ELS is located in region 2 at ρ_s = 7.746 mm.

pronounced as the ELS is moved closer to the DNG shell, e.g., to ρ_s = 5.99 mm, where the dipolar mode is excited most strongly. This stronger excitation of the dipolar mode as the ELS is moved closer to the DNG shell is also responsible for the increased symmetry in the total field, which, for example, is present in Figure 6b. These near-field results are consistent with several of the concepts reported by *Engheta and Alú* [2005].

[32] If the ELS is located in regions 2 or 3, the near fields have a dipolar form when the ELS is located near the surfaces of the DNG shell. This indicates that the maximum PR shown in Figure 3 is a result of the ELS exciting a resonant dipolar mode. When the ELS is in region 3 and is moved further away from the DNG shell, its ability to couple strongly to the dipolar mode is gradually suppressed. This explains the behavior shown in Figure 3c.

[33] As revealed by Figure 3b, the PR of the resonant DPS-DNG structure is altered significantly as the ELS is moved through region 2. In particular, no enhancement is found for ρ_s = 7.746 mm. The near field for this particular location is depicted in Figure 7 where a monopolar form is observed at large distances. Thus, as noted earlier in connection with the PR results, the ability of the ELS to excite the dipolar mode in this resonant DPS-DNG structure changes significantly as it is moved though the DNG shell, and is, in fact, lost when the ELS is located at ρ_s = 7.746 mm. The observation of the monopolar mode for that particular ELS location is rather interesting since the present DPS-DNG structure was designed specifically to excite the dipolar mode as the dominant one. This suggests that when the ELS location is close to this critical value, the near field is a mixture of the dipolar and the stronger monopolar mode. The strong presence of the monopolar mode results in the reduced enhancement of the radiated power observed in Figure 3b. Similar gradual transformations of the near field have been observed in Figures 5a and 5b for the ELS locations close to the origin. These gradual transformations of the pattern as the position of the ELS is changed in the different regions will be analysed further in section 4.2.3.

[34] Before closing this section, the following observations are in order. The results in Figure 6 show that the near fields for ρ_s = 1.0 mm and ρ_s = 5.99 mm are very similar to each other. This means that once the resonant dipolar mode is excited, its form is almost unaffected by the location of the ELS, and therefore it constitutes the natural dipolar mode of the structure. Therefore, in order to have such a mode dominate the behavior, the ELS must be placed at locations where the field is maximum, which is why it is excited most strongly when the ELS is near the surfaces of the DNG shell. On the other hand, it is very weakly excited, or not excited at all, if the ELS is placed at locations for which the field of the dipolar mode is minimum and, hence, the coupling to that mode is minimized. Among others, these low dipolar field locations are found near the origin, as well as inside region 2. More specifically, the minimum for region 2, e.g., in Figure 6a, is attained at ρ = 7.801 mm, while that in Figure 6b is attained at ρ = 7.755 mm. These values are very close to ρ_s = 7.746 mm at which the minimum PR was found for the ELS locations inside region 2. This confirms that the excitation of the dipolar mode is very weak for such ELS locations. This behavior also explains why the monopolar mode is dominant, and hence no enhancement of the total power is found, when the ELS is located at positions where the near field of the dipolar mode is very low. Moreover, it is interesting to note that additional numerical results, not included here, for the corresponding scattering problem indicate that the pure dipolar field (i.e., not mixed with the monopolar field excited by the ELS) has an exact zero at the location where the minimum of the dipolar excitation is attained inside region 2, i.e., at ρ = 7.746 mm. Similar observations also apply for the quadrupolar (and even higher order) structures considered later in this manuscript.

4.2.3. Directivity

[35] Having demonstrated, both analytically and numerically, the possibility of designing electrically small resonant MTM-based structures, where the resonant effects in such structures were explained in terms of the excitation of a given resonant mode as the dominant one, it is next of interest to examine the radiation patterns of such structures. Figure 8a shows the directivity

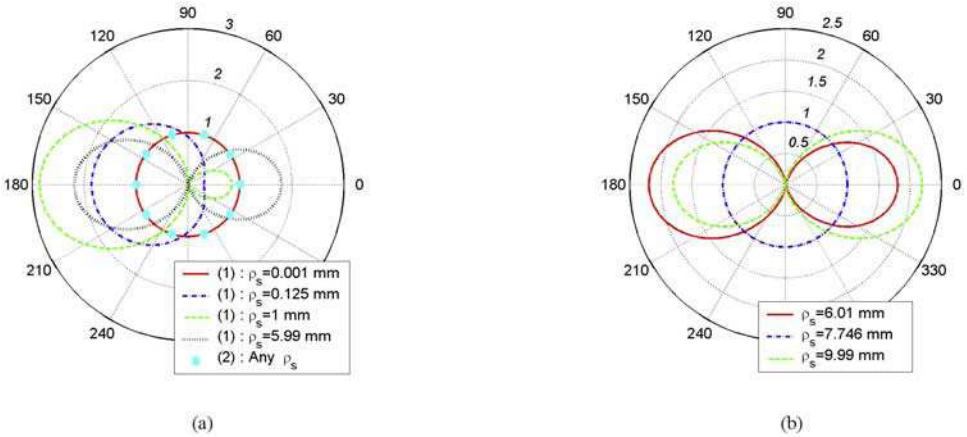

Figure 8. Directivity for various ELS locations (a) in region 1 for both DPS-DPS (labeled by (2)) and DPS-DNG structures (labeled by (1)) and (b) in region 2 for only DPS-DNG structures.

patterns for a number of ELS locations for the DPS-DNG and DPS-DPS structures.

[36] For the DPS-DNG structure, these directivity results are in agreement with the near-field results presented above. In particular, close to the origin, i.e., for $\rho_s = 0.001$ mm, the structure acts as an omnidirectional radiator and the directivity pattern is monopolar. However, for $\rho_s = 0.125$ mm, the directivity has a form which is a mixture of more modes, and the maximum directivity, $D_{\max}$, which is attained in the $\phi = 180°$ direction, equals $D_{\max} = 1.86$. For $\rho_s = 1.0$ and 5.99 mm, the directivity takes on the dipolar form, although it is not symmetric, and the maximum directivities, likewise attained in the $\phi = 180°$ direction, are $D_{\max} = 2.86$ and $D_{\max} = 2.15$, respectively. It is observed that the asymmetry in the pattern is reduced and is accompanied with the reduction of the maximum directivity, as the location of the ELS is moved towards the DNG shell. In comparison, the directivity of the corresponding DPS-DPS structure has a monopolar form, regardless of the ELS location. Thus, apart from enhanced PR values, an electrically small resonant dipolar DPS-DNG cylindrical structure provides one with the possibility of reshaping the pattern from the monopolar form to the dipolar one by changing the location of the ELS. It is interesting to note that these concepts of obtaining higher directivity with specific MTM-based structures were also investigated by *Engheta and Alú* [2005].

[37] When the ELS is in region 2, a dipolar pattern is found for the DPS-DNG structures when the ELS is located near either of the surfaces of the DNG shell, with $D_{\max} = 2.19$, while the directivity has a perfectly monopolar form for $\rho_s = 7.746$ mm. This behavior is illustrated in Figure 8b and is in agreement with the PR and near-field results. It is linked to the previously mentioned gradual transition from the dipolar to the monopolar and back to the dipolar mode of radiation. This behavior is further illustrated in Figure 9a, where the directivity is given for various ELS locations slightly to the left and right of $\rho_s = 7.746$ mm, $\phi_s = 0°$. For $\rho_s = 7.5$ mm, the directivity takes on an asymmetric dipolar form for which the main lobe is in the $\phi = 180°$ direction with $D_{\max} \approx 3$, while for $\rho_s = 7.7$ mm it is a mixture of more modes with $D_{\max} \approx 2$ attained along the same direction. This is also the case for $\rho_s = 7.8$ mm. On the other hand, for $\rho_s = 8$ mm, the directivity again has a dipolar form with $D_{\max} \approx 3$ but now with the main lobe in the $\phi = 0°$ direction. Thus, the main lobe of the directivity pattern is found to be in the same direction as the displacement of the ELS from $\rho_s = 7.746$ mm. In regard to these observations of asymmetry, one also notes from Figures 8a and 9a, that with the ELS location being displaced along the x-axis, the patterns found for source locations on either sides of $\rho_s = 7.746$ mm are mirror images of each other with respect to the y-axis. The results of Figures 8a and 9b clearly illustrate how the directivity is reshaped from the dipolar to monopolar, and back to the dipolar form, this behavior being in agreement with Figure 3b. When the ELS is located in region 3 at $\rho_s = 10.1$, 15, 20 and 30 mm respectively, the directivity takes on the dipolar forms shown in Figure 9b. Within the range of ρ_s values investigated here, more power is radiated in the $\phi = 0°$ direction and the pattern becomes increasingly asymmetric as the ELS moves further away from the DNG shell.

4.2.4. Total and Differential Cross Sections

[38] When the ELS is located in region 3 and is moved infinitely far away from the cylinders, it is of interest to investigate the behavior of the differential and total cross sections, σ_d and σ_t, respectively, given by (10) and (11)

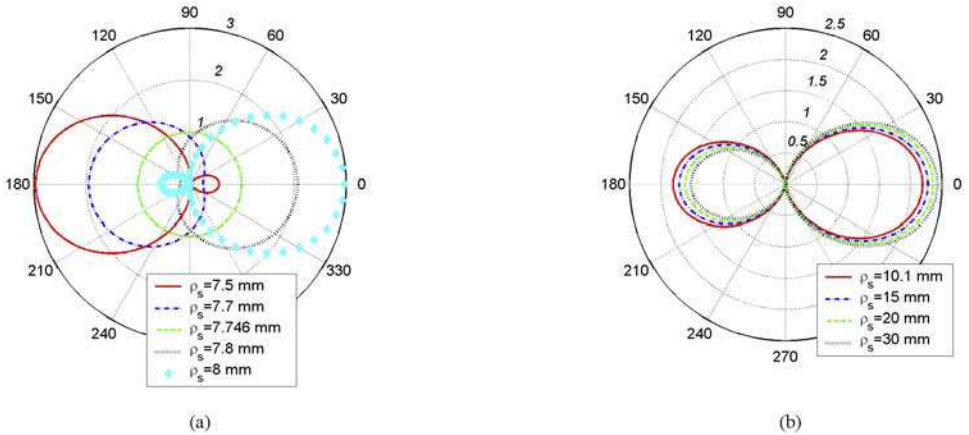

Figure 9. Directivity for DPS-DNG structures for various ELS locations around the critical value of ρ_s = 7.746 mm (a) in region 2 and (b) in region 3.

in section 2. This corresponds in practice to the situation where a TM polarized uniform plane wave is incident on the structure from the direction ϕ_s. Without loss of generality it is assumed that the location of the ELS is moved to infinity along the $\phi_s = 0$ direction.

[39] The total cross section, σ_t, or more specifically the quantity $10\log_{10}|\sigma_t|$, where σ_t has been normalized by 1 m, is shown in Figure 10 as a function of the outer radius ρ_2 when the inner radius is $\rho_1 = 6.0$ mm. Results for both the DPS-DNG and DPS-DPS structures are shown.

[40] While the total cross section of the DPS-DPS structure is very low, it is considerably enhanced by the presence of the DNG shell, in particular for the case with $\rho_2 = 10.03$ mm where a resonance peak of magnitude close to 1dB is observed even though the structure is electrically small. Furthermore, the resonance peaks observed in the PR and total cross section figures occur for the same DPS-DNG structure. With the terminology introduced by *Ziolkowski and Kipple* [2005] for the corresponding sphere case, these radiating and scattering systems are said to be reciprocal.

[41] The differential cross section is depicted in Figure 11 for the DPS-DNG and DPS-DPS structures. Both patterns have a "pure" dipolar form since the differential cross section is determined only by the scattered field terms. However, the differential cross section of the resonant DPS-DNG structure is found to be considerably larger (the maximum σ_d is $\sigma_{d,\max} = 2.54$) than that of the corresponding DPS-DPS structure (where $\sigma_{d,\max} = 4.88 \times 10^{-6}$).

[42] In concluding this section, it is interesting to note that if the same order of magnitude of σ_t and σ_d produced by the electrically small resonant dipolar DPS-DNG structure investigated above is to be obtained by a DPS-DPS structure having the same material parameters and inner radius, its outer radius ρ_2 would have to be increased approximately 20 times. This implies that the electrically small resonant dipolar DPS-DNG structure exhibits characteristics generally attributed to larger scatterers.

4.3. Electrically Small Quadrupolar Structures

[43] In this section, the radiation and scattering properties of the electrically small resonant quadrupolar DPS-DNG structure defined in section 4.1 are examined and compared to the corresponding DPS-DPS structure.

[44] Figure 12a shows the PR as a function of the outer radius ρ_2 for the quadrupolar DPS-DNG and DPS-DPS

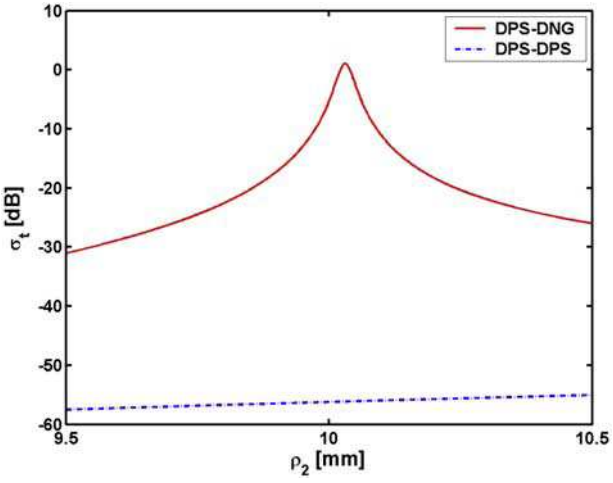

Figure 10. The total cross section σ_t as a function of the outer shell radius ρ_2 for the dipolar DPS-DNG and DPS-DPS structures.

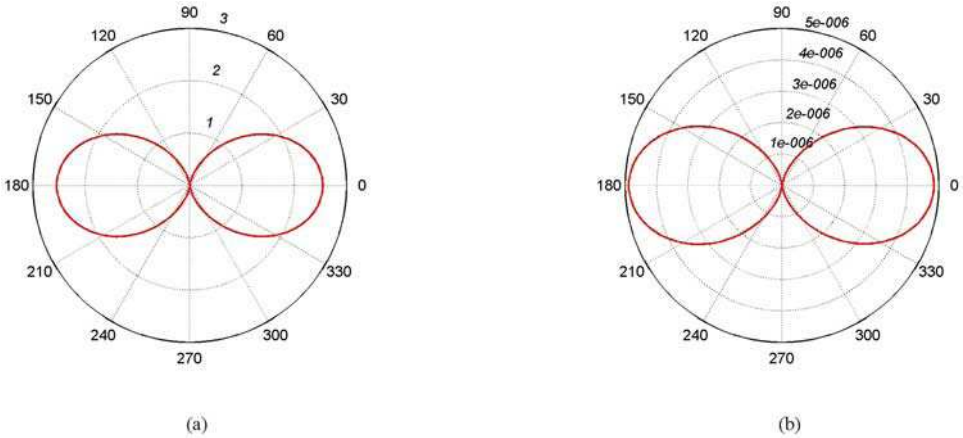

Figure 11. The differential cross section σ_d for the dipolar (a) DPS-DNG and (b) DPS-DPS structures. Note that the scale in Figure 11b has a very small dynamic range.

structures. The ELS is located in region 1 at $\rho_s = 3.8$ mm. As for the dipolar mode, the location of the ELS is chosen near the DPS-DNG interface because it produces the largest PR. Resonance, and thus the enhancement of the total power, is indeed observed in Figure 12a for the DPS-DNG structure with $\rho_2 = 5.000068$ mm. This value is very close to the approximate value of 5 mm listed in Table 2. For this resonant structure, the maximum obtainable PR is approximately 55 dB. In comparison to the dipolar case, the enhancements for the quadrupolar case are significantly larger, but the resonance is also extremely narrow and very sensitive to even very slight changes in the material and the geometrical parameters. Figure 12a also shows that no enhancements of the total power are obtained for the corresponding DPS-DPS structure.

[45] In order to confirm that these enhancements of the total power are indeed due to the resonant excitation of the quadrupolar mode of the DPS-DNG structure with $\rho_2 = 5.000068$ mm, the electric near field for this DPS-DNG structure when the ELS located at $\rho_s = 3.8$ mm is illustrated in Figure 12b. Indeed the near field in this case has the quadrupolar form, thus demonstrating that this mode is indeed the dominant one. Moreover, the near-field values of the field in a given direction in Figure 12b are notably larger than the corresponding

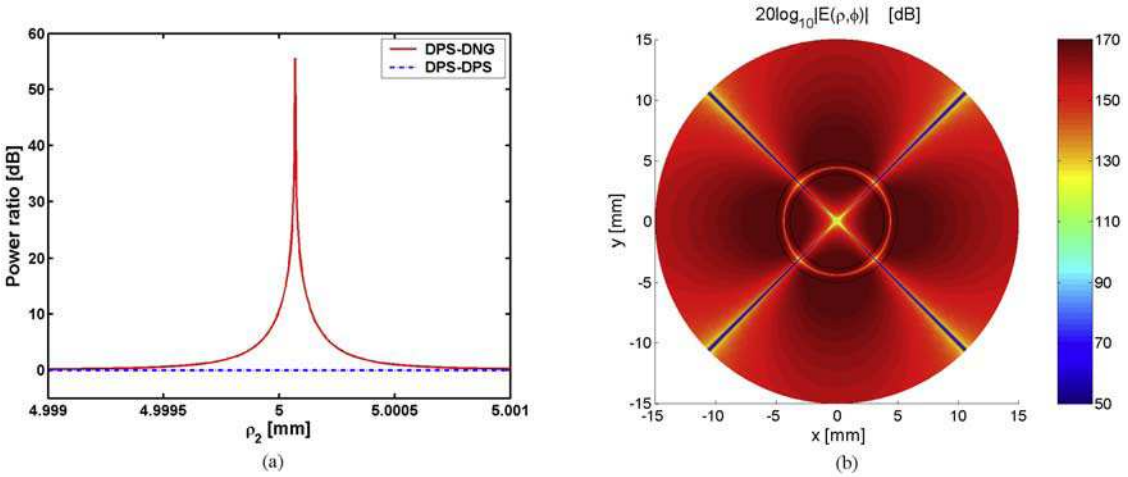

Figure 12. (a) Power ratio as a function of the outer shell radius ρ_2 for the quadrupolar DPS-DNG and DPS-DPS structure. (b) Electric near field of the resonant quadrupolar DPS-DNG structure. In both Figures 12a and 12b, the ELS is located in region 1 at $\rho_s = 3.8$ mm. Figure 12a appeared in the work of *Arslanagic et al.* [2006e].

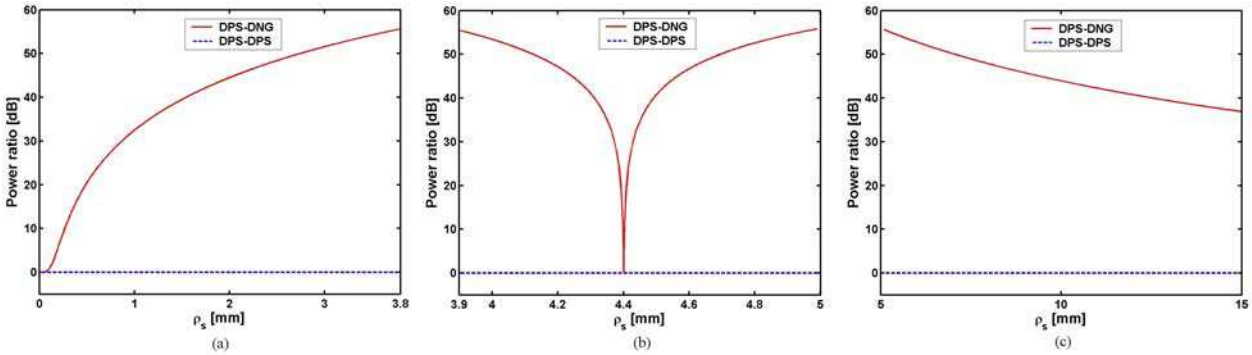

Figure 13. Power ratio as a function of the ELS location ρ_s for the DPS-DNG and DPS-DPS quadrupolar structures when the ELS is located in (a) region 1, (b) region 2, and (c) region 3. Figure 13b appeared in the work of *Arslanagic et al.* [2007]. Copyright © 2007 IEEE.

near-field values for the dipolar DPS-DNG structure, see Figure 6b. This also explains why the PR values are higher for the quadrupolar than for the dipolar DPS-DNG structure. Results similar to those reported in Figure 12 are obtained for the same quadrupolar DPS-DNG and DPS-DPS structures when the ELS is located in regions 2 and 3.

[46] As with the resonant dipolar structures discussed in section 4.1, it is of interest to examine the influence of the ELS location on the PR produced by the quadrupolar structures. To this end, Figures 13a–13c show, respectively, the PR as a function of the ELS position, ρ_s, in regions 1, 2, and 3 for the DPS-DNG and DPS-DPS quadrupolar structures having the fixed radii: ρ_1 = 3.8729 mm and ρ_2 = 5.000068 mm. In particular, the ELS location varies in the interval $\rho_s \in [1-3.8]$ mm for Figure 13a, in $\rho_s \in [3.9-4.99]$ mm for Figure 13b, and in $\rho_s \in [5.1-15]$ mm for Figure 13c.

[47] It is found that the DPS-DPS quadrupolar structures offer no enhancement, while the corresponding DPS-DNG structures offer very large values of the PR, this being particularly true when the ELS is located near the surfaces of the DNG shell. Moreover, it is clear that as the ELS location changes in the three regions, the behavior of the PR for the DPS-DNG quadrupolar structures is similar to that found in Figure 3 for the corresponding dipolar structures. Therefore, only the main distinctions between the dipolar and quadrupolar cases will be made in the following. In particular, it is found that the enhancements of the total power reported in Figure 13, reaching peak values as high as PR $\approx$ 55 dB for the ELS locations near the interfaces between the regions, are considerably higher than the PR $\approx$ 23 dB obtained for the dipolar structures. The existence of a sharp minimum in the quadrupolar DPS-DNG structure also exists, as Figure 13b confirms, in similitude with the dipolar DPS-DNG structure. Furthermore, the ability of the ELS to excite the dominant resonant mode changes significantly as its location is moved through the DNG shell. As for the resonant dipolar DPS-DNG structure, the change in the ELS location has a direct impact on the PR values as well as the shape of the near-fields and the directivity. Specifically, no enhancement of the total power is found for ρ_s = 4.400486 mm. This is due to the fact that for this location of the ELS, the monopolar mode is dominant. (With reference to the remarks at the end of section 4.2.2, the excited quadrupolar mode is likewise a natural mode of the structure in the sense that its form is basically unaffected by the ELS locations. Thus, placing the ELS at locations where the field is very low will not excite this mode. With reference to Figure 12a, these low field locations are, amongst others, near the origin as well as inside region 2 in a very narrow annular region centered on the radius ρ = 4.4 mm.) This is confirmed by the results given in Figure 14 which shows the directivity for a number of ELS locations in region 2 for the DPS-DNG structure.

[48] While the directivity has a symmetric quadrupolar form (with $D_{\max} \approx 2$) when the ELS location is close to the DNG surfaces, it has a symmetric, and rather directive, dipolar form (with $D_{\max} \approx 2.5$) with the main lobes along the y - and x -axes, respectively, when the ELS is just to the left (e.g., at ρ_s = 4.3999 mm) and right (e.g., at ρ_s = 4.401 mm) of ρ_s = 4.400486 mm. Moreover, when the ELS is located at ρ_s = 4.400486 mm, a clear monopolar pattern is produced. This explains the null in the PR results shown in Figure 13b. These pattern results demonstrate that it is possible to achieve a gradual transformation of the directivity from the quadrupolar to the dipolar to the monopolar form, and back again, as the ELS is moved through the DNG shell. The details of this transformation are illustrated in Figure 15, where the directivity is shown for ELS locations near ρ_s = 4.3999 mm, ρ_s = 4.400486 mm, and ρ_s = 4.401 mm, respectively, in

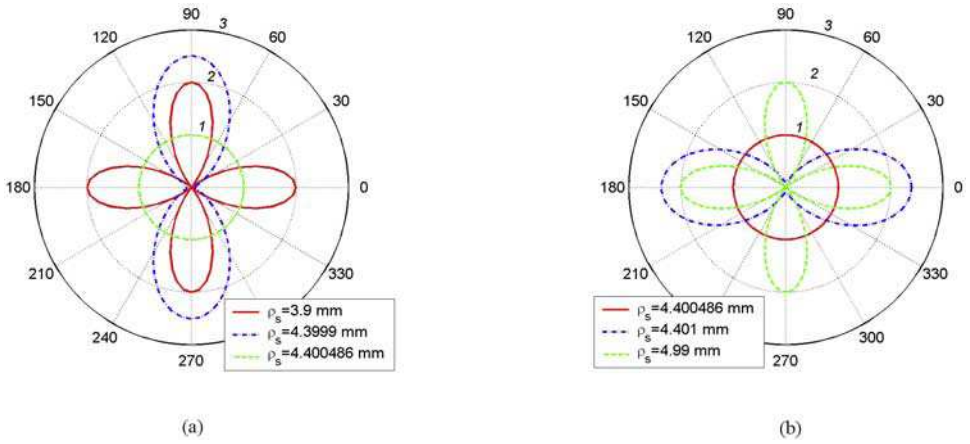

Figure 14. Directivity for various ELS locations in region 2 for the resonant DPS-DNG quadrupolar structure.

Figures 15a–15c. It is interesting to observe that rather directive beams with $D_{\max} \approx 2.9$ are found in Figures 15a and 15c.

[49] The pattern variations shown in Figure 15 are in agreement with the PR values reported in Figure 13b. They serve as a confirmation that a particular resonant mode must be excited to achieve enhancements of the total radiated power. It is important to emphasize that not only can one control the modal form of the directivity pattern with the DPS-DNG quadrupolar structure, but one can also control the direction of the enhancement. The change between the vertical and horizontal dipolar patterns as the ELS is located at specific positions confirms this behavior. The gradual transformations from the monopolar to the dipolar to the quadrupolar mode of radiation are also found when the ELS location moves in region 1 from the origin toward the DNG shell. Thus, the quadrupolar structure, as compared to the dipolar one, offers an additional mode of radiation and, thus, an additional degree of freedom in controlling the pattern through the movement of the ELS location.

[50] In the case of the ELS being moved infinitely far away from the structure along the direction $\phi_s = 0$, the total cross section, σ_t, or more specifically the quantity $10\log_{10}|\sigma_t|$, where, as before, σ_t has been normalized by 1 m, attains the form shown in Figure 16 for the DPS-

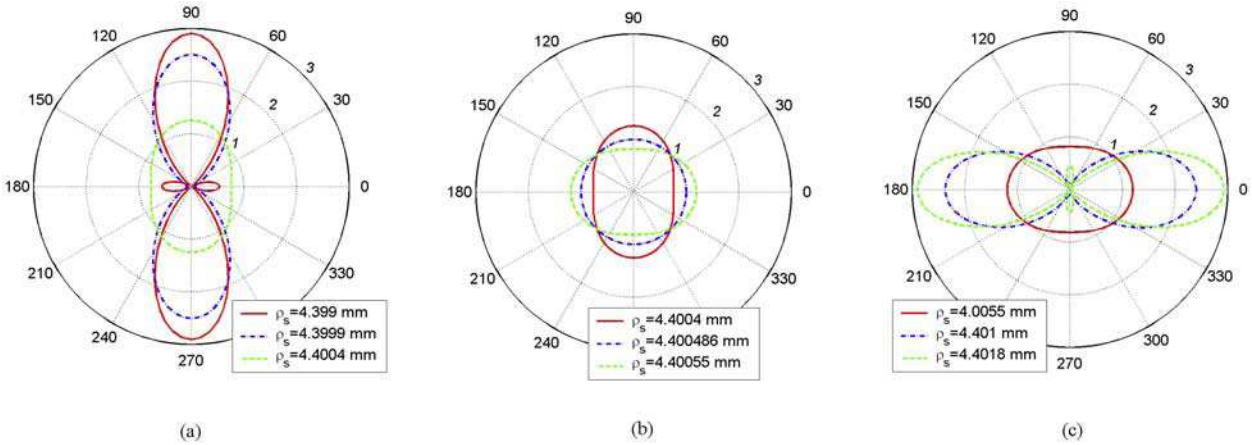

Figure 15. The changes in the directivity as the ELS location is varied in region 2 of the DPS-DNG structure: (a) to the left of the critical radius, (b) near and at the critical radius, and (c) to the right of the critical radius [from *Arslanagic et al.*, 2007]. Copyright © 2007 IEEE.

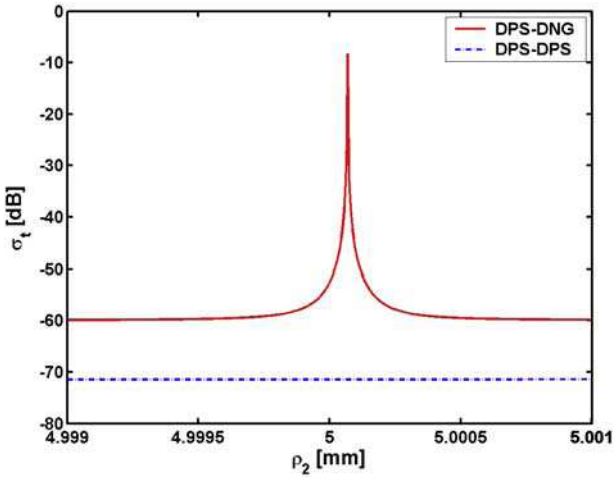

Figure 16. The total cross section σ_t as a function of the outer shell radius ρ_2 for the electrically small resonant quadrupolar DPS-DNG and DPS-DPS structures.

DNG and DPS-DPS structures. As shown, a resonant enhancement is observed at $\rho_2 = 5.000068$ mm (which is indeed the same ρ_2 value at which the resonance was observed in the PR values), while no enhancement is found for the corresponding DPS-DPS structure. In addition, at the radius for which the resonance is achieved for the quadrupolar DPS-DNG structure, the difference between σ_t for the DPS-DNG and DPS-DPS structures is larger for the quadrupolar structures than for the dipolar ones. Although not included here, significant enhancements of the differential cross section were obtained for the resonant quadrupolar DPS-DNG structure relative to the corresponding DPS-DPS structure.

5. Effects of Dispersion and Losses

[51] To assess the effects of dispersion and losses on the resonant behavior of the DPS-DNG structures, the well-known Drude and Lorentz models of both the permittivity and permeability were used. The lossy Drude model of the permittivity and permeability are given, respectively, by the expressions

$$\varepsilon_2(\omega) = \varepsilon_0\left(1 - \frac{\omega_{pe}^2}{\omega(\omega - j\Gamma_e)}\right), \tag{13a}$$

$$\mu_2(\omega) = \mu_0\left(1 - \frac{\omega_{pm}^2}{\omega(\omega - j\Gamma_m)}\right), \tag{13b}$$

while the lossy Lorentz model of the permittivity and permeability are given, respectively, by the expressions

$$\varepsilon_2(\omega) = \varepsilon_0\left(1 - \frac{\omega_{pe}^2}{\omega^2 - j\Gamma_e\omega - \omega_{er}^2}\right), \tag{14a}$$

$$\mu_2(\omega) = \mu_0\left(1 - \frac{\omega_{pm}^2}{\omega^2 - j\Gamma_m\omega - \omega_{mr}^2}\right). \tag{14b}$$

[52] In the above relations ω_{pe} and ω_{pm} are the electric and magnetic plasma frequencies, while Γ_e and Γ_m are the electric and magnetic collision frequencies. In the Lorentz models, ω_{er} and ω_{mr} are the resonance frequencies of the permittivity and permeability, respectively. These models were designed to recover at the angular frequency of operation, $\omega_0 = 2\pi f_0$ with $f_0 = 300$ MHz, the values of the lossless permittivity and permeability given in Table 2. For the Drude models, the values of ω_{pe}^2 and ω_{pm}^2 are determined, respectively, from the real part of (13a) and (13b) evaluated at ω_0 to recover the desired material parameter values. For the Lorentz models, with the assumption that the losses are small, the frequency of operation f_0 must lie above the resonance frequency to obtain the required negative values of the material parameters. Since the resonant angular frequencies of the Lorentz model permittivity and permeability are given by $\omega_{er} = 2\pi f_{er} = \omega_{mr} = 2\pi f_{mr} = 2\pi f_r$, we set $f_r = 290$ MHz and then determine the values of ω_{pe}^2 and ω_{pm}^2 from the desired values of the real parts of (14a) and (14b).

[53] For both models, the following two cases are considered. In the first case, the collision frequencies are set to zero, i.e., $\Gamma_e = \Gamma_m = 0$. This means the DNG shell is lossless but dispersive. In the second case, the collision frequencies are set to $\Gamma_e = \Gamma_m = 10^{-3}\ \omega_0$. This means the DNG shell is dispersive and contains a small but nonnegligible loss. The effects of dispersion and losses on the performance of the electrically small resonant dipolar DPS-DNG structures examined in section 4.2 are shown in Figure 17.

[54] The general characteristics of these results are that the PR is almost constant in the depicted frequency range when the DNG shell is nondispersive, and thus these structures are rather broadband. This broadband behavior is expected since the electrical size of the dipolar DPS-DNG structure is small for the range of frequencies considered in Figure 17a, and thus the resonance condition in (12) holds for all of these frequencies. On the other hand, the results clearly show that when dispersion is introduced into the DNG shell, the bandwidth of the resonance attained at $f_0 = 300$ MHz is narrowed considerably. The Lorentz model results have a much narrower

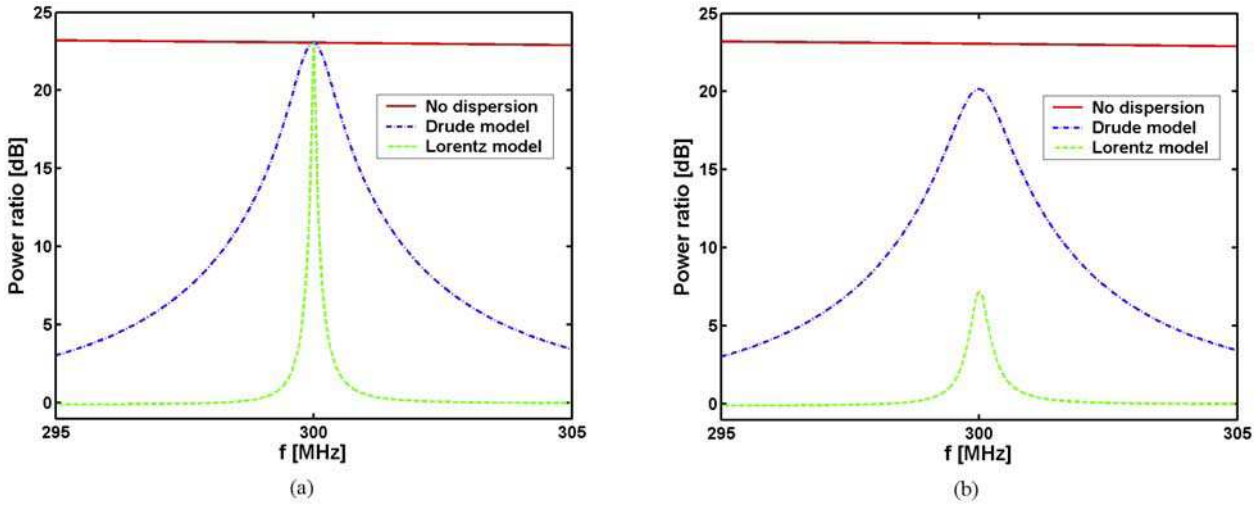

Figure 17. PR as a function of the frequency for the DPS-DNG cases in which the DNG shell is described by a nondispersive model and by the Drude and Lorentz dispersion models with (a) $\Gamma_e = \Gamma_m = 0$ and (b) $\Gamma_e = \Gamma_m = 10^{-3}\ \omega_0$. The ELS is located in region 1 at $\rho_s = 5.99$ mm. Figure 17a appeared in the work of *Arslanagic et al.* [2006e]. Copyright © 2006 Wiley Periodicals, Inc.

bandwidth than those obtained with the Drude model, this being particularly the case when the two dispersion models are lossless, see Figure 17a. The narrower bandwidth in the Lorentz model case is explained by the fact that this model is itself resonant, and thus its material parameters exhibit rapid variations near f_0 = 300 MHz. Furthermore, it is interesting to note that the maximum value of the PR obtained with either lossless dispersion model occurs at f_0 = 300 MHz and is the same value obtained in the nondispersive case. The inclusion of loss in the two dispersion models has basically two effects. First, as Figure 17b shows, the resonances in the PR still occur at f_0 = 300 MHz, but they are somewhat broadened relative to the two lossless dispersive cases considered in Figure 17a. Second, the maximum value of the PR obtained with either lossy dispersion model is lower that in the nondispersive case. In particular, the PR values evaluated at f_0 = 300 MHz are PR = 23.05 dB for the nondispersive case, PR = 20.16 dB for the lossy Drude model, and PR = 7.18 dB for the lossy Lorentz model. Thus, the decrease in the amplitude of the PR is most profound for the lossy Lorentz dispersion model. This behavior is expected since the loss is more severe in the Lorentz model (even though the same collision frequencies were used as in the Drude model) because there is a resonance and the frequency of operation is near to the resonance frequency. In particular, for the indicated model parameters, one finds at f_0 = 300 MHz that $\varepsilon_2 = \varepsilon_0\,(-1 - \mathrm{j}0.002)$, $\mu_2 = \mu_0\,(-4 - \mathrm{j}0.005)$ for the Drude model, and that $\varepsilon_2 = \varepsilon_0\,(-1 - j0.03)$ $\mu_2 = \mu_0\,(-4 - j0.07)$ for the Lorentz model. Thus, the electric and magnetic loss tangents: $LT_e = \varepsilon_2''/|\varepsilon_2'|$ and $LT_m = \mu_2''/|\mu_2'|$, are, respectively, $LT_e = 0.002$, $LT_m = 0.00125$ (Drude model) and $LT_e = 0.03$, $LT_m = 0.0175$ (Lorentz model). Similar results, not included here, have been obtained for the dipolar DPS-DNG structures for which the ELS is located in regions 2 and 3.

[55] The effects of losses on the performance of the DPS-DNG structures are further investigated by assuming that the DNG shell is lossy but dispersionless. To this end, five lossy cases, for which the permeabilities and magnetic loss tangents are evaluated at f_0 = 300 MHz, are summarized in Table 3. Only the magnetic loss is included since, as shown in section 4, it is the permeability, and not the permittivity, of the DNG shell that determines the overall behavior for this TM case. (Note that very large electric loss will have a strong impact on the results reported here. However, as long as the electric loss is comparable to the magnetic loss considered here, it can be neglected.) In Figure 18a, the PR is shown for the five lossy cases as a function of the ELS location when it is in region 2. The lossless case, treated in section 3, is likewise included for reference purposes. As observed in Figure 18a, the PR curve is broadened and the total power enhancements are diminished as the losses are increased. While a small amount of loss (Cases 1 and 2) has little impact on the PR values, a moderate amount of loss (Case 3) significantly influences the enhancement of the total power. In Case 3 the maximum PR is half (in dB) of the lossless case value. However, it is only after the inclusion of very large losses (Cases 4 and 5) that very small or practically no enhancements

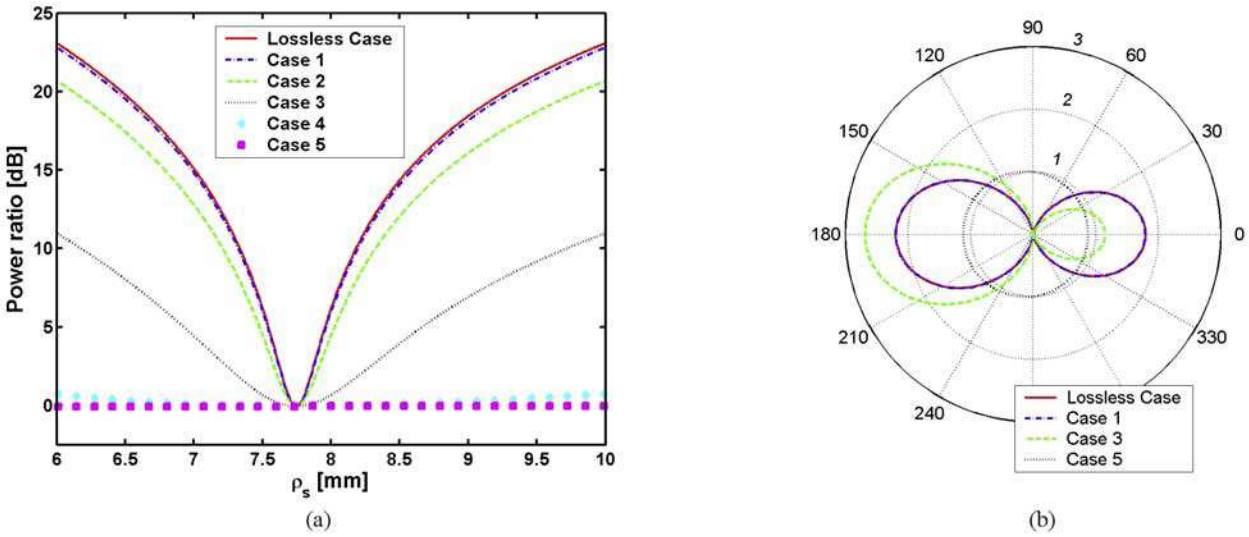

Figure 18. Influence of the losses on the dipolar DPS-DNG structure: (a) PR as a function of the ELS location ρ_s in region 2, and (b) the directivity when the ELS is located at ρ_s = 6.01 mm. The lossless dipolar DPS-DNG structure is included for reference purposes.

occur. The decrease in the PR values as the losses increase is due to the fact that the inclusion of losses gradually suppresses the excitation of the resonant higher order modes and, hence, favors the monopolar mode. This is confirmed by the directivity results given in Figure 18b. One finds that while Case 1 has essentially the same directivity as the lossless case and Case 3 still retains a dipolar form of the directivity, Case 5 actually produces a directivity pattern that is dominated by the monopolar mode. Additional investigations, not included here, have revealed that the inclusion of even larger magnetic losses produces a perfect monopolar pattern. It is noted that the results related to the influence of loss on the performance of the resonant DPS-DNG structure investigated here are consistent with those reported by *Engheta and Alú* [2005].

[56] Note that only the results for the resonant dipolar DPS-DNG structures have been presented. It must be stressed that similar effects occur when the resonant quadrupolar and higher-order DPS-DNG structures are considered. Although not included in this manuscript, it has been shown that these structures have significantly narrower bandwidths and are even more sensitive to the inclusion of dispersion and small losses.

6. Wavelength-Sized Natural Resonances

[57] It was noted above that very electrically small concentric MTM cylinders with the ELS located exactly at the origin can not lead to total power enhancements because the ELS is only able to excite the monopolar mode and none of the higher-order modes that are required for these enhancements. Nonetheless, it is important to mention that with sufficiently large DPS- and DNG-based structures, the wavelength-sized natural resonances of those structures can be excited. They occur when the size of the object is comparable to multiples of the wavelength [*Alú and Engheta*, 2003a, 2005]. To illustrate this point, it is sufficient to investigate DPS-DPS and DPS-DNG structures having the same material parameters given in Table 2 but with larger radii. As above, the frequency of operation is f_0 = 300 MHz; and the ELS is located at the origin, i.e., ρ_s = 0 mm. The inner radius of region 2 is fixed at ρ_1 = 10 mm, and the outer one is allowed to vary in the interval $\rho_2 \in [10, 300]$ mm. Figure 19 shows the behavior of the PR as a function of ρ_2. Clearly, both the DPS-DPS and DPS-DNG structures exhibit resonances even though the ELS is located on the axis. It is clear that these resonances are of the monopolar type since, as mentioned in section 3, only the monopolar mode radiates when the ELS is located at the origin.

[58] For the DPS-DPS structure the resonance is attained at ρ_2 = 178.49 mm and for the DPS-DNG

Table 3. Five Lossy Cases for the Additional Investigation on the Effects of Loss

Parameter	Case 1	Case 2	Case 3	Case 4	Case 5
μ_2/μ_0	−4 − j0.0004	−4 − j0.004	−4 − j0.04	−4 − j0.4	−4 − j4
LT_m	0.0001	0.001	0.01	0.1	1

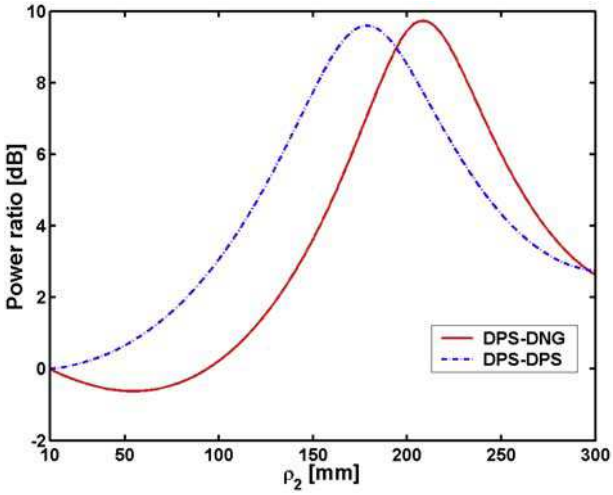

Figure 19. PR as a function of the outer shell radius ρ_2 for the DPS-DNG and DPS-DPS cylindrical structures when the ELS is located on the axis of the cylinders. The values of ρ_2 are allowed to be large enough to capture the wavelength-sized natural resonances [from *Arslanagic et al.*, 2006e]. Copyright © 2006 Wiley Periodicals, Inc.

structure at ρ_2 = 208.36 mm. The maximum value is PR = 9.59 dB for the DPS-DPS structure, and PR = 9.72 dB for the DPS-DNG structure. These results show that when the size of the cylinders is in the natural resonance regime, the DPS-DNG structures do not offer any advantage over the corresponding DPS-DPS structures. This is in agreement with the results given by *Khodier* [2004] and *Nelatury* [2006]. This conclusion holds in fact for all locations of the ELS. This is in sharp contrast to the very electrically small MTM structures treated in this paper, which were found to have natural resonances that were caused by pairing ordinary DPS materials with specific MTMs and that led to the significant performance enhancements.

[59] The wavelength-sized natural resonance phenomenon is familiar from waveguide and cavity theories where the natural modes occur if the structure has certain dimensions [e.g., see *Balanis*, 1989]. In particular, for TM polarization in an open circular dielectric resonator of radius a and wave number k, the first resonance occurs at ka = 1.84 [*Balanis*, 1989].

7. SNG Structures

[60] Although this manuscript has emphasized the use of DNG and DPS materials, a brief note on the use of SNG media, such as ENG or MNG media, is important. In section 4 it was noted that electrically small resonant structures having the same properties as the DPS-DNG structures could be designed by using only MNG materials. This is due to the fact that the resonance condition (12) only includes the permeability of the three regions, and not the permittivity. Thus it can also be met simply with DPS-MNG structures. This is very interesting, particularly from a practical point of view, since a DPS-MNG structure may be much simpler to realize than the corresponding DPS-DNG one. Therefore, it is of interest to examine a configuration consisting of an ELS radiating in the presence of a DPS-MNG dipolar structure. The DPS-MNG dipolar structure introduced here has the same material and geometrical parameters as the DPS-DNG dipolar structure considered in section 3, except that now the permittivity of region 2 is positive and equal to $\varepsilon_2 = \varepsilon_0$. For the sake of completeness, a DPS-ENG structure is likewise considered; it also has the same material and geometrical parameters as the DPS-DNG dipolar structure, except that now the permeability of region 2 is positive and equal to $\mu_2 = 4\mu_0$.

[61] Figure 20 shows the PR as a function of the outer radius ρ_2 for the DPS-MNG and DPS-ENG dipolar structure when the ELS is located in region 1 at ρ_s = 5.99 mm. A resonance peak with PR ≈ 23 dB is found in the PR values at ρ_2 = 10.033 mm, which is extremely close to the value at which the resonance was attained for the dipolar DPS-DNG structure. On the other hand, the PR for the corresponding DPS-ENG structure exhibits no enhancement of the total power; thus it resembles the behavior of the DPS-DPS structure. This confirms that a

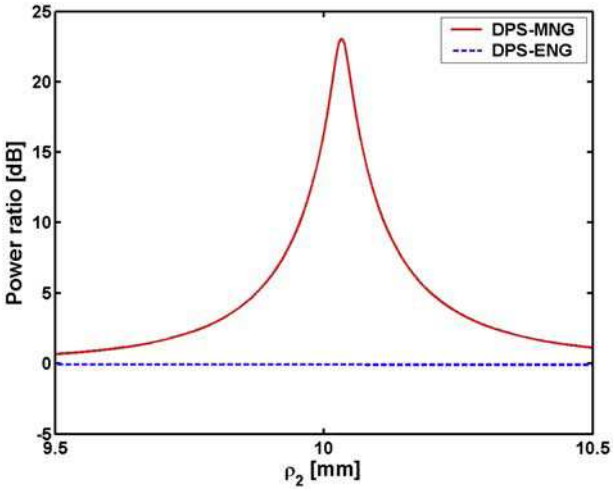

Figure 20. PR as a function of the outer shell radius ρ_2 for the dipolar DPS-MNG and DPS-ENG structures when the ELS is located in region 1 at ρ_s = 5.99 mm.

DPS-MNG structure can indeed replace the DPS-DNG structure while a DPS-ENG structure can not. It must be stressed that the underlying mechanism for the enhancement of the total power by the DPS-MNG structures is identical to that occurring in the DPS-DNG structure. As a consequence, the behavior of the near field, directivity, and total and differential cross sections of the DPS-MNG structures resembles that of the DPS-DNG structures, as does the influence of dispersion and losses present in MNG materials.

[62] Another interesting point regards the use of TE polarization (e.g., with a magnetic line source), instead of the present TM polarization. In the TE case it can be shown that the resonance condition (12) includes the permittivity of the three regions, and not the permeability. Consequently, for the TE case it will be an ENG material, rather than a MNG one that will provide a structure whose behavior is similar to the DPS-DNG and DPS-MNG structures treated here.

[63] It must also be noted that when the ELS is located at the origin of a DPS-MNG structures whose size is comparable to that of the DPS-DPS and DPS-DNG structures discussed in section 6 and for which resonances were obtained at $\rho_2 = 178.49$ mm and at $\rho_2 = 208.36$ mm, respectively, no enhancements of the total power can be observed. The explanation is straightforward. When the ELS is located at the origin, only the monopolar mode radiates. As discussed in section 6, the size of the structure must be sufficiently large in order to obtain a resonance. However, for such a large DPS-MNG structure, the MNG shell will be quite thick. Consequently, this shell will not permit the passage of electromagnetic waves since the wave number inside it is imaginary; and thus the waves are evanescent rather than propagating in the shell [*Engheta and Ziolkowski*, 2006, chapter 2]. Thus, no enhancements will result for DPS-MNG structures of that large size. Having the ELS displaced from the origin leads to enhancements only in the case where the DPS-MNG structure is electrically small, as well as in the case where the structure is electrically large and the MNG shell is simultaneously thin.

8. Conclusions

[64] An antenna configuration consisting of an arbitrarily located ELS radiating in the presence of concentric MTM cylinders was solved analytically and investigated numerically for the particular case of either a DPS or a DNG shell. The near- and far-field properties of these structures were analysed through an investigation of various parameters including the total radiated power, directivity, and total and differential cross sections. The results for these MTM-based structures were compared to the corresponding structures made of conventional DPS materials.

[65] In summary, it was shown that the electrically small MTM-based structures can be designed to possess resonances in the radiation and scattering characteristics, whereas such resonances do not exist for the corresponding DPS-based structures. In particular, significant enhancements of the total radiated power, as compared to the power radiated by the ELS in free space, as well as the total and differential cross section, were found by using specifically designed electrically small DPS-DNG structures. These enhancements were associated with the so-called subwavelength-sized natural resonances, also referred to as interface resonances in the work of *Alú and Engheta* [2003a], that may occur in such small structures. The main characteristic of these enhancements, which are found for off-axis ELS locations, is that they are considerably larger when the ELS is located near the interfaces of the DNG layers, where it can directly drive these resonances. Both dipolar and quadrupolar resonant structures were designed, and the enhancements for the quadrupolar ones were shown to be significantly larger than those for the dipolar ones, but the resonances were also shown to be narrower, and more sensitive to even slight variations of the material as well as the geometrical parameters.

[66] For both the dipolar and quadrupolar structures, the feasibility of controlling the directivity of the electrically small MTM-based structures through specific locations of the ELS was demonstrated. Even though a given resonant MTM-based structure was designed to be excited in a specific dominant mode, other modes can be excited by proper locations of the ELS. Thus, it is possible to reshape the pattern to obtain desired radiation characteristics.

[67] Frequency dispersion in the MTM material was shown to narrow the resonances significantly, while the inclusion of losses in the dispersion models decreased the peak values of those resonances. In addition, a separate analysis revealed that while small and moderate losses in the MTMs do not the make the enhancement of the quantities of interest disappear, large losses do so, this being caused by the suppressed excitation of the necessary higher order modes.

[68] It was furthermore demonstrated that MNG, like DNG, materials can offer the same results for the ELS excitation (TM polarization) of these cylindrical structures, while it was noted that for the TE polarization case, e.g., obtained by using a magnetic line source excitation, ENG (or DNG) materials must be used. These observations on the use of SNG rather than DNG materials to realize the electrically small resonant structures are important, especially from the practical point of view, since the manufacturing of a SNG material may be easier than that of a DNG material.

[69] It is worth emphasizing that the electrically small DPS-DNG structures investigated here possess enhanced

radiation and scattering characteristics that are similar to those associated with an electrically large structure. When the size of the MTM-based structure is large enough for the wavelength-sized natural resonances to occur, it was shown that both the DPS-DNG and DPS-DPS structures (but not the DPS-SNG structures) possess resonances in the total radiated power, although smaller in amplitude, even when the ELS was located on the axis of the cylinders.

[70] **Acknowledgment.** This work was supported in part by DARPA contract HR0011-05-C-0068.

References

Abramowitz, M., and I. A. Stegun (1965), *Handbook of Mathematical Functions*, Dover, Mineola, N. Y.

Alú, A., and N. Engheta (2003a), Resonances in subwavelength cylindrical structures made of pairs of double-negative and double-positive or epsilon-negative and mu-negative coaxial shells, paper presented at International Conference on Electromagnetics in Advanced Applications, Turin, Italy, 8–12 Sept.

Alú, A., and N. Engheta (2003b), Pairing an epsilon-negative slab with a mu-negative slab: resonance, tunneling, and transparency, *IEEE Trans. Antennas Propag.*, *51*, 2558–2571.

Alú, A., and N. Engheta (2005), Polarizabilities and effective parameters for collections of spherical nano-particles formed by pairs of concentric double-negative (DNG), single-negative (SNG) and/or double-positive (DPS) metamaterial layers, *J. Appl. Phys.*, *97*, 094310.

Arslanagic, S., and O. Breinbjerg (2006), Electric line source illumination of a circular cylinder of lossless double negative material – an investigation of near field, directivity and radiation resistance, *IEEE Antennas Propag. Mag.*, *48*, 38–54.

Arslanagic, S., R. W. Ziolkowski, and O. Breinbjerg (2006a), Radiated power and total scattering cross section of multilayered cylinders excited by an electric line source, paper presented at Third Workshop on Metamaterials and Special Materials for Electromagnetic Applications and TLC, Rome, Italy.

Arslanagic, S., R. W. Ziolkowski, and O. Breinbjerg (2006b), Line source excitation of multilayered metamaterial cylinders: source and scattering results, paper presented at Antennas and Propagation Society Symposium, Inst. of Electr. and Electron. Eng., Albuquerque, N. M.

Arslanagic, S., R. W. Ziolkowski, and O. Breinbjerg (2006c), Hertzian dipole excitation of higher order resonant modes in electrically small concentric metamaterial spheres: source and scattering structures, paper presented at IV International Workshop on Electromagnetic Wave Scattering, Gebze, Turkey.

Arslanagic, S., R. W. Ziolkowski, and O. Breinbjerg (2006d), Near-field distribution, directivity and differential scattering cross section for a line source-excited metamaterial-coated electrically small cylinder, paper presented at European Conference on Antennas and Propagation (EuCap), Nice, France.

Arslanagic, S., R. W. Ziolkowski, and O. Breinbjerg (2006e), Excitation of an electrically small metamaterial-coated cylinder by an arbitrarily located line source, *Microwave Opt. Technol. Lett.*, *48*, 2598–2605.

Arslanagic, S., R. W. Ziolkowski, and O. Breinbjerg (2007), Far-field properties of a line source-excited electrically small quadrupolar metamaterial cylindrical shell, paper presented at International Workshop on Antenna Technology (iWAT), Cambridge, England.

Balanis, C. A. (1989), *Advanced Engineering Electromagnetics*, John Wiley, Hoboken, N. J.

Caloz, C., and T. Itoh (Eds.) (2006), *Electromagnetic Metamaterials—Transmission Line Theory and Microwave Applications*, John Wiley, Hoboken, N. J.

Eleftheriades, G. V., and K. G. Balmain (Eds.) (2005), *Negative-Refraction Metamaterials—Fundamental Principles and Applications*, John Wiley, Hoboken, N. J.

Engheta, N., and A. Alú (2005), Can negative-parameter metamaterials provide high directivity for small aperture antennas, paper presented at Digest of USNC/URSI National Radio Science Meeting, Washington, D. C.

Engheta, N., and R. W. Ziolkowski (Eds.) (2006), *Metamaterials—Physics and Engineering Explorations*, John Wiley, Hoboken, N. J.

Khodier, M. M. (2004), Radiation characteristics of an infinite line source surrounded by concetric shells of metamaterials, paper presented at Antennas and Propagation Society Symposium, Inst. of Electr. and Electron. Eng., Monterey, Calif.

Kuzmiak, V., and A. A. Maradudin (2002), Scattering properties of a cylinder fabricated from a left-handed material, *Phys. Rev. B.*, *66*, 1161–1167.

Li, C., and Z. Shen (2003), Electromagnetic scattering by a conducting cylinder coated with metamaterials, paper presented at Progress in Electromagnetic Research Society Meeting, PIERS'03, Honolulu, Hawaii.

Liu, Z., Z. Lin, and S. T. Chui (2004), Electromagnetic scattering by spherical negative-refractive-index particles: Low frequency resonance and localization parameters, *Phys. Rev. E.*, *69*, 016 619/1-6.

Nelatury, S. R. (2006), Comparing double-negative and double-positive covers around a radiating line current, *Microwave Opt. Technol. Lett.*, *48*, 250–252.

Pendry, J. B. (2000), Negative refraction makes a perfect lens, *Phys. Rev. Lett.*, *85*, 3966–3969.

Ruppin, R. (2000), Extinction properties of a sphere with negative permittivity and permeability, *Solid State Commun.*, *116*, 411–415.

Ruppin, R. (2004), Surface polaritons and extinction properties of a left-handed cylinder, *J. Phys., Condens. Matter*, *16*, 5991–5998.

Sun, J., W. Sun, T. Jiang, and Y. Feng (2005), Directive electromagnetic radiation of a line source scattered by a

conducting cylinder coated with left-handed material, *Microwave Opt. Technol. Lett.*, *47*, 274–279.

Tretyakov, S. A., S. I. Maslovski, A. A. Sochava, and C. R. Simovski (2005), The influence of complex material coverings on the quality factor of simple radiating systems, *IEEE Trans. Antennas Propag.*, *53*, 965–970.

Veselago, V. G. (1968), The electrodynamics of substances with simultaneously negative values of ε and μ, *Sov. Phys. Usp.*, *10*, 509–514.

Ziolkowski, R. W., and A. Erentok (2006), Metamaterial-based efficient electrically small antennas, *IEEE Trans. Antennas Propag.*, *54*, 2113–2130.

Ziolkowski, R. W., and A. Erentok (2007), At and beyond the Chu limit: Passive and active broad bandwidth metamaterial-based efficient electrically small antennas, *IET Microwave Antennas Propag.*, *1*, 116–128.

Ziolkowski, R. W., and A. Kipple (2003), Application of double negative metamaterials to increase the power radiated by electrically small antennas, *IEEE Trans. Antennas Propag.*, *51*, 2626–2640.

Ziolkowski, R. W., and A. Kipple (2005), Reciprocity between the effects of resonant scattering and enhanced radiated power by electrically small antennas in the presence of nested metamaterials shells, *Phys. Rev. E.*, *72*, 036602.

S. Arslanagic and O. Breinbjerg, Ørsted·DTU, Electro-Science, Technical University of Denmark, Building 348, Ørsteds Plads, DK-2800 Kgs. Lyngby, Denmark. (sar@oersted.dtu.dk)

R. W. Ziolkowski, Department of Electrical and Computer Engineering, University of Arizona, 1230 E. Speedway Blvd., Tucson, AZ 85721-0104, USA.